ARMY RESEARCH LABORATORY

Effect of Strain Rates on the Compressive Response of Neck Rubber From Humanetics HIII 50th Percentile Male Dummy Under Different Loading Sequences

by Brett Sanborn, Paul Moy, Randy Mrozek, and Tusit Weerasooriya

ARL-TR-6336 **February 2013**

NOTICES

Disclaimers

The findings in this report are not to be construed as an official Department of the Army position unless so designated by other authorized documents.

Citation of manufacturer's or trade names does not constitute an official endorsement or approval of the use thereof.

Destroy this report when it is no longer needed. Do not return it to the originator.

Army Research Laboratory
Aberdeen Proving Ground, MD 21005-5069

ARL-TR-6336 **February 2013**

Effect of Strain Rates on the Compressive Response of Neck Rubber From Humanetics HIII 50th Percentile Male Dummy Under Different Loading Sequences

Brett Sanborn
Oak Ridge Institute for Science and Education (ORISE)

Paul Moy, Randy Mrozek, and Tusit Weerasooriya
Weapons and Materials Research Directorate, ARL

REPORT DOCUMENTATION PAGE	Form Approved OMB No. 0704-0188

1. REPORT DATE *(DD-MM-YYYY)*	2. REPORT TYPE	3. DATES COVERED (From - To)
February 2013	Final	July 2012–January 2013

4. TITLE AND SUBTITLE
Effect of Strain Rates on the Compressive Response of Neck Rubber From Humanetics HIII 50th Percentile Male Dummy Under Different Loading Sequences

5a. CONTRACT NUMBER
1120-1120-99

5b. GRANT NUMBER

5c. PROGRAM ELEMENT NUMBER

6. AUTHOR(S)
Brett Sanborn,* Paul Moy, Randy Mrozek, and Tusit Weerasooriya

5d. PROJECT NUMBER

5e. TASK NUMBER

5f. WORK UNIT NUMBER

7. PERFORMING ORGANIZATION NAME(S) AND ADDRESS(ES)
U.S. Army Research Laboratory
ATTN: RDRL-WMP-B
Aberdeen Proving Ground, MD 21005-5069

8. PERFORMING ORGANIZATION REPORT NUMBER
ARL-TR-6336

9. SPONSORING/MONITORING AGENCY NAME(S) AND ADDRESS(ES)

10. SPONSOR/MONITOR'S ACRONYM(S)

11. SPONSOR/MONITOR'S REPORT NUMBER(S)

12. DISTRIBUTION/AVAILABILITY STATEMENT
Approved for public release; distribution is unlimited.

13. SUPPLEMENTARY NOTES
* ORISE, 4692 Millennium Drive, Suite 101, Belcamp, MD 21017

14. ABSTRACT
Anthropomorphic test dummies (ATDs) are used to understand the response of humans exposed to different possible extreme loading scenarios encountered as occupants of automotives, aircraft, and military vehicles. The Warrior Injury Assessment Manikin (WIAMan) program has been established by the U.S. Army to create a higher fidelity ATD that will be used to assess severity of injury to humans in blast and high accelerative loading situations, where loading rates could be higher than during the standard automotive crash tests. Simulation of these extreme events to extract the accurate response of ATDs requires incorporating the constitutive response of the materials used in the ATDs under different loading rates. To build constitutive models for numerical codes for WIAMan, the materials used in ATDs must be investigated to discover how the materials behave at various loading rates. In this study, the rate-dependent behavior of neck rubber used in the Hybrid III, an automotive ATD, was investigated over quasi-static (0.001 s^{-1}), intermediate (1 s^{-1}), and high (500 s^{-1}, 1300 s^{-1}, and 2300 s^{-1}) strain rates. The stress relaxation behavior at quasi-static and intermediate rates was also studied. In addition, storage and loss moduli of the rubber were also obtained as a function of frequency and temperature. These various types of loading under different rates were used to evaluate the various representations of constitutive models in literature. The Bergstrom-Boyce model was identified as the model that best represents the experimental data.

15. SUBJECT TERMS
SHPB, rubber response, Hybrid III, neck, high rate, Bergstrom-Boyce, stress-strain, loading rate, ATD, humanetics, constitutive modeling

16. SECURITY CLASSIFICATION OF:			17. LIMITATION OF ABSTRACT	18. NUMBER OF PAGES	19a. NAME OF RESPONSIBLE PERSON
a. REPORT	b. ABSTRACT	c. THIS PAGE			Brett Sanborn
Unclassified	Unclassified	Unclassified	UU	42	19b. TELEPHONE NUMBER (*Include area code*) 410-306-4925

Standard Form 298 (Rev. 8/98)
Prescribed by ANSI Std. Z39.18

Contents

List of Figures

Acknowledgments

The authors would like to acknowledge the valuable discussions with Dr. Jorgen Bergstrom during the calibration simulation process to obtain Bergstrom-Boyce material model constants. We would also like to acknowledge the effort from scientists at Humanetics, Dr. Hyunsok Pang and Dr. Jerry Wang, to fabricate the neck rubber material at appropriate thicknesses for high-rate experiments. Without their efforts, we would not be able to conduct valid high-rate experiments at all, including this valuable study for the high-priority Warrior Injury Assessment Manikin (WIAMan) project. We would also like to thank Randy Coates for his support for this research for us to demonstrate our novel approaches for this problem.

1. Introduction

Anthropomorphic test dummies (ATDs) are used as test devices by automotive and aircraft industries and regulatory bodies and the military to evaluate vehicle safety in crash environments. Early designs of ATDs only required that the size and weight be similar to their human counterparts, whereas more modern ATDs are designed to assess type and severity of injury and to mimic human response in these dynamic environments (*1*).

Several iterations of ATDs have been made throughout the past 70 years in an attempt to more closely approximate the response of humans in dynamic environments, such as auto crashes. The earliest ATD was used in 1949 to investigate the effects of ejection seats. The first ATD used in automotive compliance testing was the Hybrid II (HII), designed in 1972 by General Motors. The HII featured high repeatability, durability, human-like shape and weight, and realistic motion for some joints and was instrumented to measure head, chest, and pelvic accelerations, and femoral loads. In 1976, the HII was further improved and renamed as Hybrid III (HIII). The HIII is differentiated from the HII by a curved lumbar spine and a biofidelic neck, head, chest, and knees for blunt and knee impact response. The HIII has an improved measurement capability over the HII as there are 44 measurement locations on the HIII ATD compared to a few for the HII (*1*).

While the HIII dummy is an adept tool for collecting data and measuring accelerative loads in automotive and aerospace crash situations, there is a need for an ATD to measure accelerative loads at even higher loading rates, such as those encountered by Soldiers in vehicles during mine blasts. The Warrior Injury Assessment Manikin (WIAMan) program has been established to understand the requirements for an ATD that will be used in these high-loading rate scenarios and to develop a new ATD to elucidate human response to blast loads. To develop constitutive models for numerical simulation of the ATDs, the materials used in these devices must be investigated to understand how the material in ATDs behaves at elevated loading rates.

The split-Hopkinson pressure bar (SHPB) has been used extensively to study the high-rate behavior of rubber materials. Chen et al. (*2*) developed a technique to measure weak signals associated with soft materials, such as the material studied in this work. Song and Chen (*3*) studied the relationship between specimen length and stress equilibration on a room-temperature vulcanizing silicone rubber. In different works, they provided techniques for loading soft materials in dynamic hysteretic loops (*4*) and studied the rate dependence of ethylene propylene diene monomer (EPDM) rubber under high-rate uniaxial compression using an SHPB (*5*). Additionally, Song and Chen used a strain energy-based function to describe a one-dimensional constitutive relation to describe the high strain rate behavior of the EPDM rubber, which agreed with the experimental results over the range of strains and strain rates. Lee et al. (*6*) conducted

experiments to obtain the compressive stress-strain behavior of a nitrile rubber under dynamic compression.

In the current study, the strain rate dependence of the butyl neck rubber material used in a typical HIII dummy has been investigated over a wide range of compressive loading rates from quasi-static (0.001 s^{-1}) and intermediate (1 s^{-1}) up to loading rates in the SHPB regime (500 s^{-1}, 1300 s^{-1}, and 2300 s^{-1}). The stress relaxation behavior of the rubber was also characterized at quasi-static and intermediate rates. In addition, the response of the rubber under small amplitude vibratory loading condition was also studied under different frequencies to obtain the storage and loss moduli as a function of loading frequency. The results from all experiments were used to explore the ability of most available constitutive models to describe the behavior of the rubber.

2. Experiments

A Bose Electroforce setup was used to determine the quasi-static and intermediate rate behavior of the HIII neck rubber at rates of 0.001 s^{-1} and 1 s^{-1}, respectively. The rubber specimens used in this study were made of butyl rubber, with a durometer of 70–80 (*7*) taken from sheet ID no. 0001 HIII 50th Neck (H) produced on 20 September 2012 at 1:35 p.m. The thickness of the sheet was 1.55 mm.

An SHPB setup was used to determine the dynamic uniaxial stress-strain behavior of the neck rubber material. The compression test setup used solid 19.05-mm-diameter incident, transmission, and striker bars. The length of the striker was 0.6 m. Pulse shaping was used to reach a constant strain rate of deformation during the experiments. A schematic of the conventional SHPB used for high-rate experiments is shown in figure 1, and a typical oscilloscope record from a high-rate experiment is shown in figure 2.

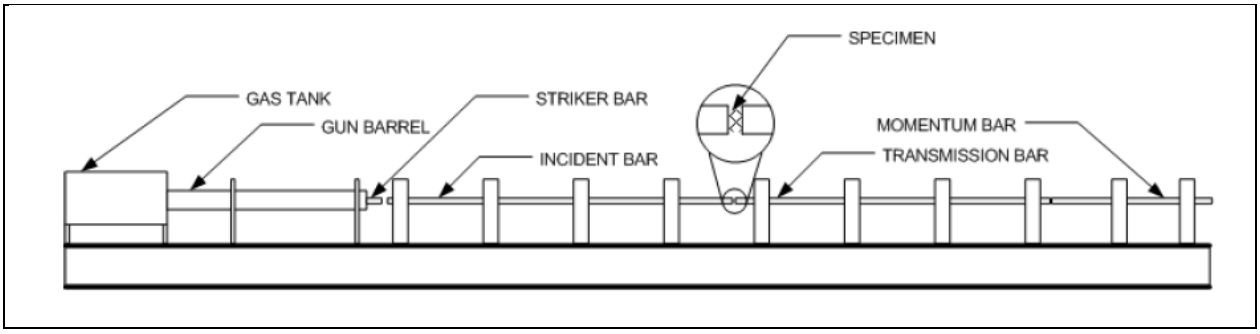

Figure 1. SHPB used for high-rate rubber experiments.

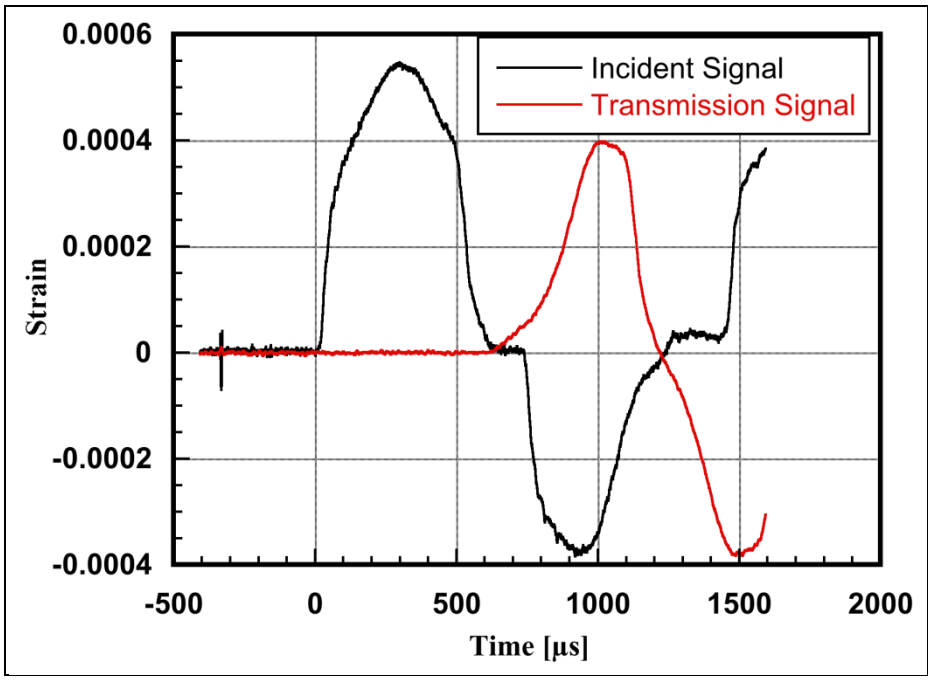

Figure 2. Oscilloscope output from a high-rate experiment on the HIII neck rubber.

For experiments with soft materials, such as rubber, quartz disks are typically embedded in the ends of the incident and transmission bars of the SHPB to check the requirement of dynamic equilibrium of the sample throughout the experiment. This quartz disk method is typically used when the compliance of the soft material is so low that nearly all of the incident pulse is reflected back. However, the stiffness of the HIII neck rubber was high enough that the dynamic equilibrium requirement could be verified using the traditional method instead of direct measurement by calculating that the forces on each end of the specimen are the same throughout the experiment, or in terms of strain in the bar,

$$\varepsilon_i + \varepsilon_r = \varepsilon_t. \tag{1}$$

Here, ε_i, ε_r, and ε_t are the incident, reflected, and transmitted waves in the bars, respectively. A typical result for the dynamic equilibrium check is shown in figure 3. The thin specimen reached dynamic equilibrium fairly early during the experiments. Both ends of the sample reached the same value early in the experiment. To reduce friction effects at the bar-specimen interface, petroleum jelly was used as a lubricant at the bar and specimen interfaces.

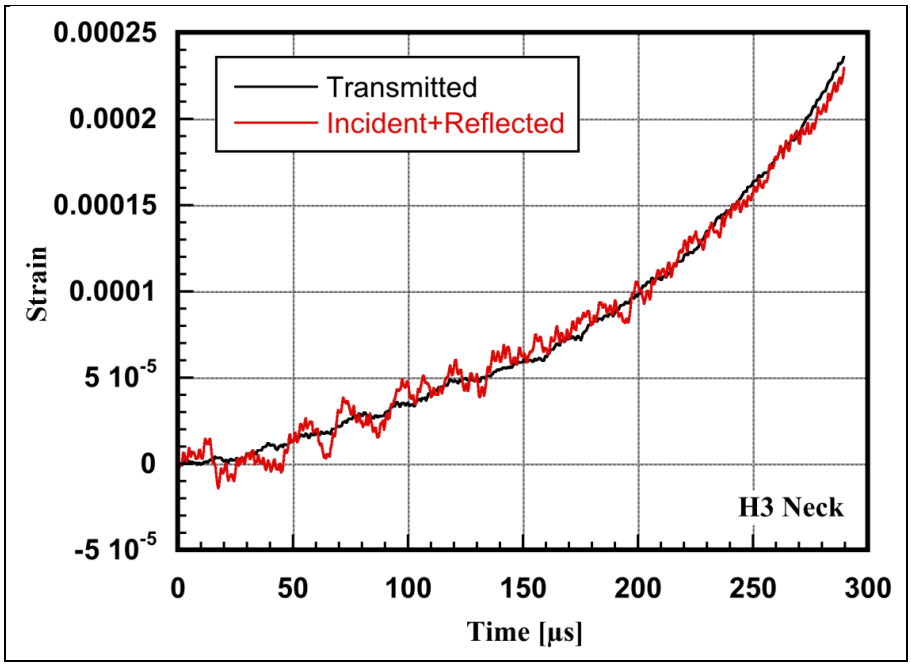

Figure 3. Strain profiles at the ends of the specimen, showing dynamic equilibrium during a high-rate experiment of the HIII neck rubber specimen.

Since rubbers are considered incompressible during deformation, the cross section of the specimen may exceed the diameter of the bars at high axial strains. Using this incompressibility assumption, which leads to constant volume of the specimen under axial compression, the maximum diameter of a sample, d_o, at a desired engineering strain is calculated using the following (5):

$$d_o = d_{bar}\sqrt{1-\varepsilon_E}\,, \tag{2}$$

where d_{bar} is the bar diameter and ε_E is the maximum engineering strain before the sample exceeds the diameter of the bars. Using equation 2, samples 8 mm in diameter and 1.55 mm in thickness were selected so that valid experiments could be conducted at engineering strains of up to 82%. This sample geometry was used for all experiments. Five experiments at each rate were conducted.

Since a traditional SHPB setup was used, the engineering stress, strain rate, and strain (taken as extension divided by original length) are calculated using the following (*8*):

$$\sigma_E = \frac{A_t}{A_s} E\varepsilon_t\,, \tag{3}$$

$$\dot{\varepsilon}_E = -2\,\frac{c_o}{L_s}\varepsilon_r, \tag{4}$$

and

$$\varepsilon_e = -2\,\frac{c_o}{L_s}\int_0^t \varepsilon_r(t)\,dt\,, \tag{5}$$

where E is the Young's modulus of the bar and, A_t and A_s are the area of the transmission bar and sample, respectively, and L_s and c_o are the length of the specimen and the wave speed in the bar. Conversions to true stress and true strain are simply made by the classical method.

When soft materials are tested at high strain rates on an SHPB, radial inertia can play a significant role in the measured response from the experiment. Warren and Forrestal (*9*) derived a relation to describe the extra stress in the measured output signal induced by radial inertia. The inertia induced stress is as follows:

$$\sigma_i = \frac{3\rho_s r^2}{16(1-\varepsilon_x)^3}\dot{\varepsilon_x}^2 + \frac{\rho_s r^2}{8(1-\varepsilon_x)^2}\ddot{\varepsilon_x}\,, \tag{6}$$

where ρ_s and r are the density and radius of the specimen and $\ddot{\varepsilon_x}$, $\dot{\varepsilon_x}$, and ε_x are the strain acceleration, strain rate, and strain in the specimen. The approximate amount of extra stress on a sample of the HIII neck rubber, assuming ρ_s = 1250 kg/m^3, ε_x = 0.58, $\dot{\varepsilon_x}$= 2300 s^{-1}, and r =4 mm, is about 0.27 MPa. As shown later in the experimental results, the measured response of the rubber is on the order of 100 MPa at this strain rate. Hence, for these experiments on the neck rubber, radial inertia effects can be ignored.

Using a Bose Electroforce experimental setup, the neck rubber was also studied at room temperature to understand the compressive response of storage (E') and loss (E") moduli as a function of frequencies from 0.1 to 100 Hz. Disk specimens 4.76 mm in diameter and 1.55 mm thick were used for these experiments. During these experiments, mean strain was kept constant at ~0.1 and strain amplitudes at ~0.0075. For each frequency, the specimen was loaded for around 20 cycles. These series of experiments provided the response of E' and E" as a function of frequency for constitutive modeling.

3. Results and Discussion

3.1 Experimental Results

3.1.1 Compressive Stress-Strain Experiments at Constant Loading Rates

3.1.1.1 Slow and Intermediate Loading Rates

The stress-strain behavior of the HIII neck rubber for quasi-static and intermediate rates is shown in figure 3. The plots shown in figure 4 represent the average behavior from five experiments at each rate. Quasi-static and intermediate rate experiments were carried out up to engineering strains of 43%. The HIII neck rubber showed a small amount of rate sensitivity when the strain rate was varied from 0.001 s^{-1} to 1 s^{-1}. The increase in flow stress was noted at about 12%, when the strain rate increased from 0.001 s^{-1} to 1 s^{-1}. The full results of all the quasi-static and intermediate rate experiments in terms of engineering stress-strain and true stress-strain plots are shown in appendix A.

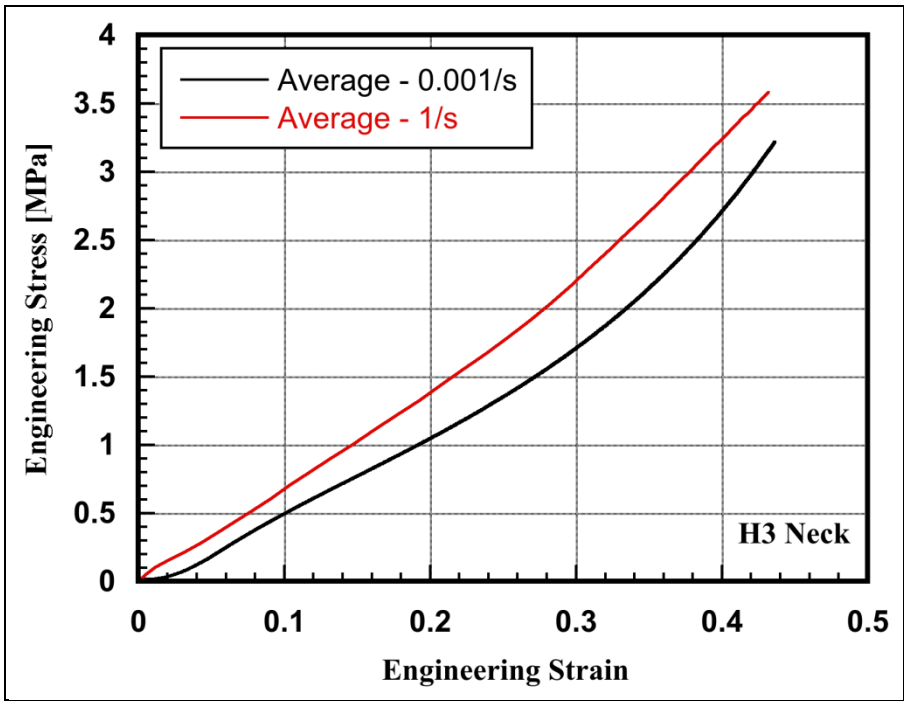

Figure 4. Engineering stress-strain behavior of the HIII neck rubber at quasi-static and intermediate rates.

3.1.1.2 High Loading Rates

Dynamic behavior of the neck rubber was determined for three strain rates: 500 s^{-1}, 1300 s^{-1}, and 2300 s^{-1}. Figure 5 shows the strain rate histories of the 2300 s^{-1} dynamic experiments; additional strain rate histories can be found in appendix A. After a rise time of 100 μs, the samples achieved constant strain rate. The neck rubber was nonlinear at the quasi-static strain rate, while a nearly linear behavior was seen at the intermediate rates. The dynamic stress-strain behavior of the rubber was averaged over the five experiments for all experimental data sets (shown in figure 5). Comparing the quasi-static and dynamic experiments, the HIII neck rubber was rate-dependent and highly nonlinear.

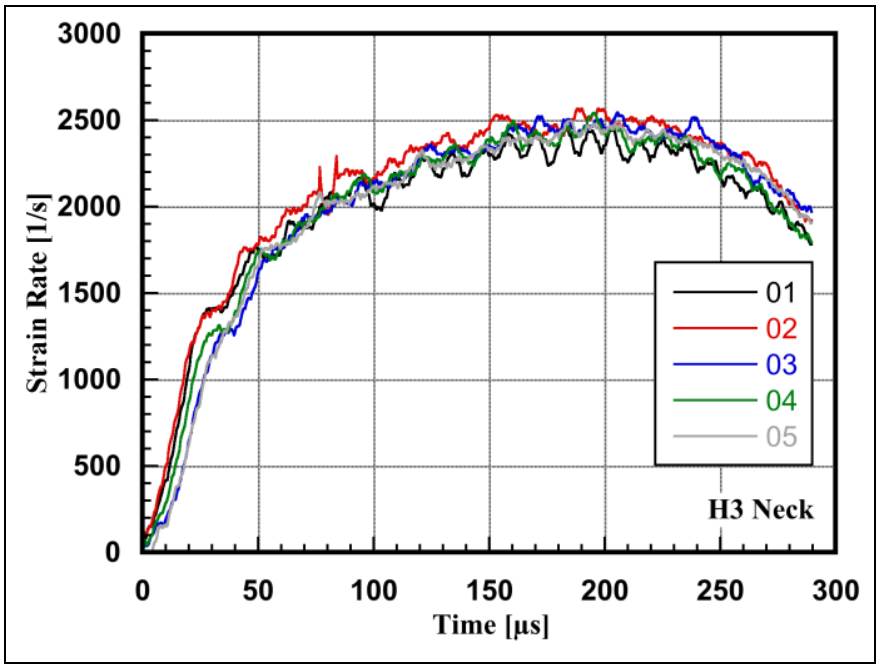

Figure 5. Strain rate histories from the 2300/s rubber experiments.

As the average behavior in figure 6 shows, the specimen responds by hardening when high axial strains are applied. Due to the limited length of the SHPB used in this study, the level of strain in the sample at intermediate rates was limited. A longer incident bar and striker were required to attain high strains at intermediate rates (*10*). Since the scale of the stress-strain response was drastically different at high rates, the high-rate and quasi-static and intermediate rate results could not be combined on the same plot. As seen in figure 3, the response of the material is about 3 MPa at quasi-static and intermediate rates at a strain of 43%; however, when the strain rate is increased to 2300 s^{-1}, the response of the material is about 57 MPa, an increase in strength of about 20. When comparing the quasi-static and intermediate rate data to the 500 s^{-1} SHPB results, the flow stress of the rubber increases from about 0.5 MPa at the quasi-static and intermediate rate to about 6 MPa at 500 s^{-1}. This behavior and rate dependence was similar to the EPDM rubber studied by Chen and Zhang (*2*), which also displayed this nonlinear and hardening behavior at elevated strain rates. Making a direct comparison, the butyl rubber used in the HIII was about 6× stronger than the EPDM rubber at the same strain (50%) and strain rate of ~2000 s^{-1}. The results of all high-rate experiments in terms of engineering stress-strain and true stress-strain are shown in appendix A.

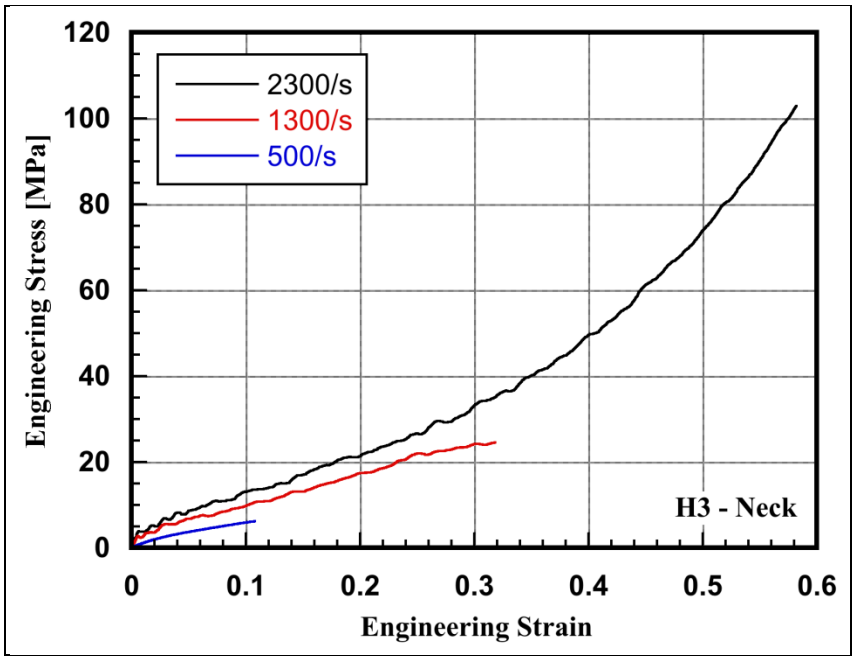

Figure 6. Engineering stress-strain behavior of the HIII neck rubber at high strain rates.

3.1.1.3 Effect of Strain Rate on the Flow Stress

Flow stress is plotted as a function of strain rate and is shown in figure 7 for strains of 0.1 and 0.2. For both strains, flow stress data can be represented by double slope curves, with a transition from one slope to the other occurring at a strain rate of ~250/s. This indicates that a single model covering strain rates from 0.001 to 2300/s does not exist, as shown later in section 3.2.

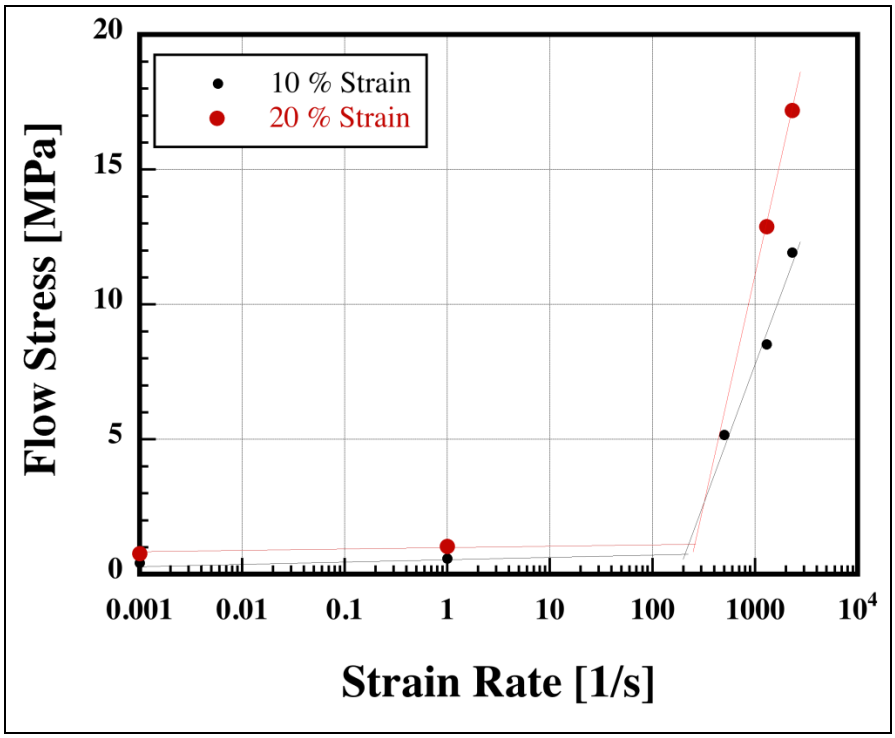

Figure 7. Flow stress as a function of strain rate at 0.1 and 0.2, showing two-slope response and transitioning from one slope to the other at ~250/s.

3.1.2 Stress Relaxation

Stress relaxation experiments were conducted at quasi-static and intermediate rates of initial loading. For both strain rates, the rubber samples were loaded and held at a constant strain of 43% for 300 s, with the exception of one experiment at the quasi-static rate held for 600 s. The stress relaxation curves at quasi-static and intermediate rates are shown in figures 8 and 9, respectively. In all cases, the HIII neck rubber displayed viscoelastic behavior, as seen by relaxation of the stress when the sample was held at a constant strain.

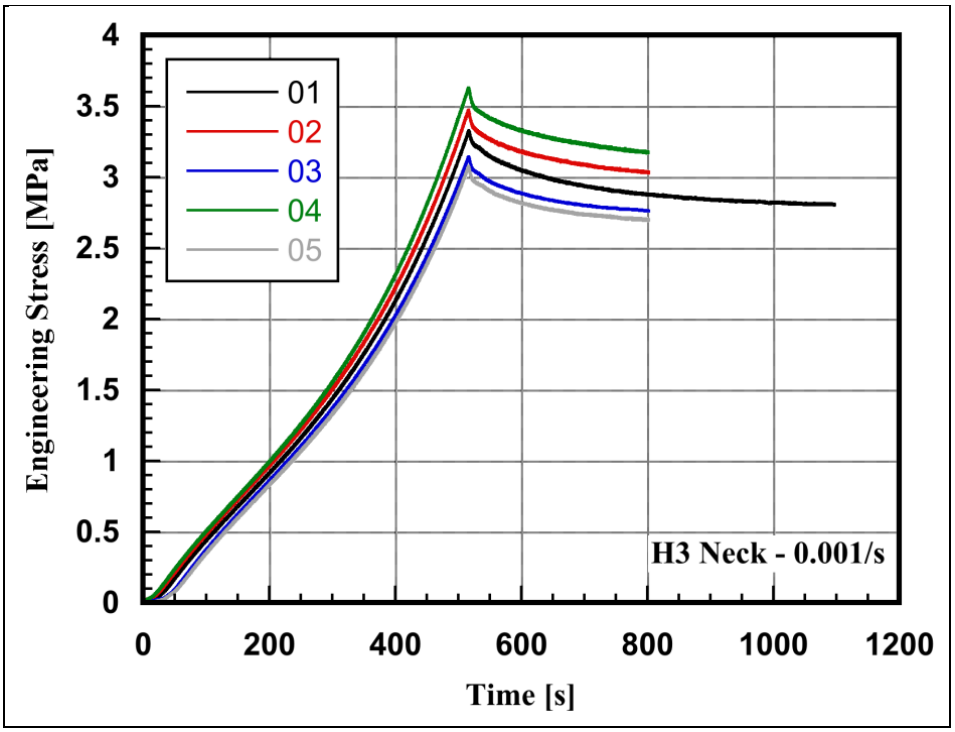

Figure 8. Stress relaxation of the HIII neck rubber at the quasi-static rate.

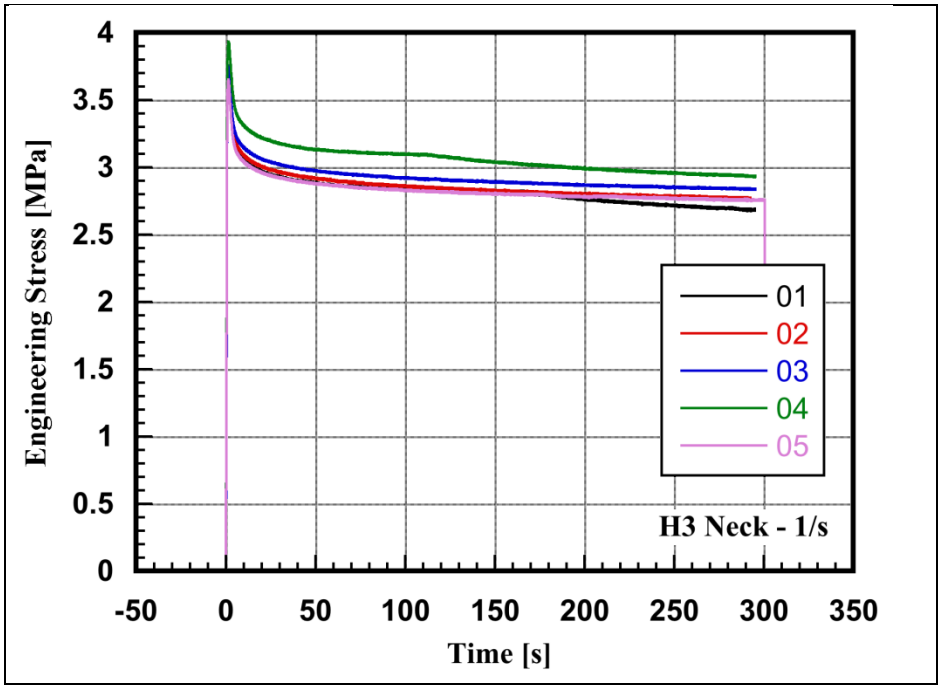

Figure 9. Stress relaxation of the HIII neck rubber at the intermediate rate.

3.1.3 Cyclic Response to Small Amplitude Loading: Storage and Loss Moduli

3.1.3.1 Uniaxial Compressive Dynamic Mechanical Analysis (DMA) Experiments at Room Temperature as a Function of Frequency

In addition to stress-strain and relaxation experiments, rubber mechanical response was also evaluated under small amplitude vibratory loading conditions over different frequencies at room temperature using DMA techniques. Storage (E') and loss (E") moduli were calculated from experimental measurements using Fourier transformation of the input and output sinusoidal loading and strain waves for each frequency. Results from these experiments are given in the table 1 and figure 10.

Table 1. DMA (E' and E") response of the neck rubber.

ε-mean	ε-amp	Frequency (Hz)	E' (MPa) (0.0075 A)	E" (MPa) (0.0075 A)	T (K)
–0.1000	0.0075	0.10	14.8	3.2	293
–0.1000	0.0077	10.12	21.6	7.3	293
–0.1000	0.0077	19.55	23.6	9.3	293
–0.1000	0.0077	29.33	25.5	10.5	293
–0.0999	0.0073	39.10	27.3	11.5	293
–0.1001	0.0077	48.88	29.1	12.2	293
–0.0998	0.0078	58.65	31.0	13.0	293
–0.0999	0.0078	70.87	32.3	13.0	293
–0.0997	0.0082	78.20	33.0	13.5	293
–0.1002	0.0082	87.98	35.3	14.4	293
–0.1002	0.0092	102.64	36.2	13.8	293

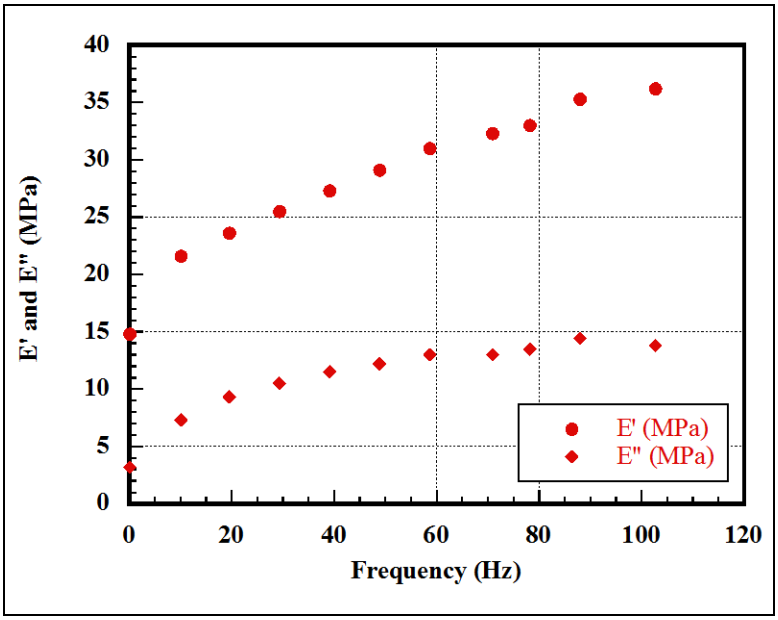

Figure 10. Storage and loss moduli as a function of the frequency of sinusoidal straining.

3.1.3.2 Uniaxial Tensile DMA Experiments at a Frequency of 1 Hz as a Function of Temperature

Tensile DMA experiments on the neck rubber were also completed over a wide temperature range (presented in figure 11). The rubber was held at a constant frequency of 1 Hz, and the temperature varied from –100 to 150 °C. The temperature DMA experiments were not used in determining the constitutive representation of the mechanical response of the material.

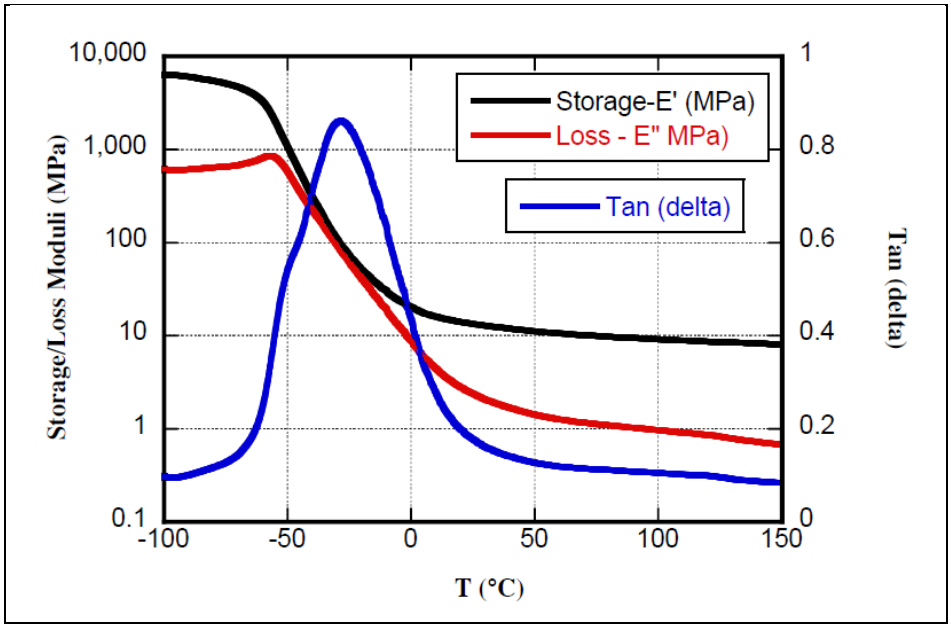

Figure 11. Results from tensile DMA experiments.

3.2 Constitutive Representation of the Mechanical Response

Various polymeric constitutive models were evaluated for their ability to represent the experimentally obtained mechanical response from different loading types and rates. The Bergstrom-Boyce (BB) model (*11*) represented most of the experimental data reasonably well.

The BB model is an advanced model to predict the time-dependent large-strain behavior of elastomeric type materials. It is based on applied deformation gradient acting on two interacting parallel macromolecular networks—A (representing equilibrium response with a hyperelastic element) and B (representing time-dependent response where hyperelastic element is in series with a time-dependent element): $\boldsymbol{F} = \boldsymbol{F}_A = \boldsymbol{F}_B$. Rheological representation of the model is given in figure 12. Deformation gradient acting on the network B, which provides the time-dependent viscous response, is further divided into elastic and viscoelastic components: $\boldsymbol{F}_B = \boldsymbol{F}_B^e \cdot \boldsymbol{F}_B^v$.

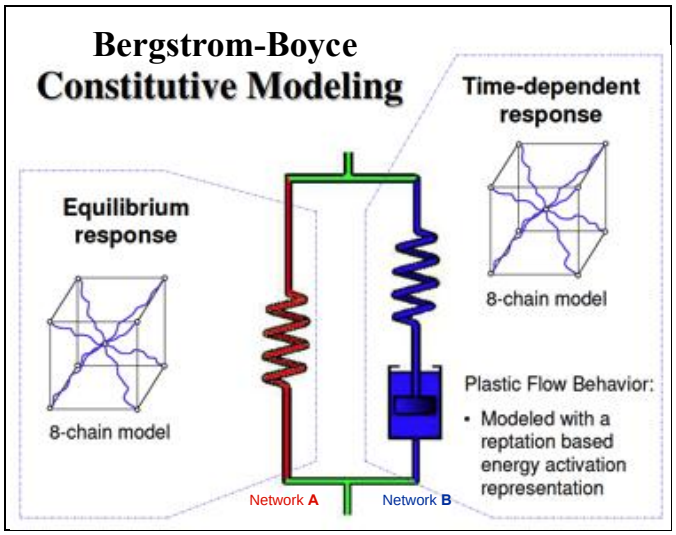

Figure 12. Rheological representation of the BB model.

In the BB model, elastic response of the two networks is given by the statistical mechanics-based, three-dimensional (3-D), eight-chain model from Arruda and Boyce (*12*) and is represented by Langevin springs in figure 8. Here, the macromolecular chains are aligned along the diagonals of the unit cell, which are assumed randomly distributed. In this representation, chains deform with the cell.

A detailed description of the 3-D theory and uniaxial simplification of the BB model can be found in Bergstrom and Boyce (*11*, *13*, and *14*). For uniaxial loading experiments in this study, the total Cauchy (true) stress is given by $\sigma = \sigma_A + \sigma_B$. Following Arruda and Boyce (*12*),

$$\sigma_A = \frac{\mu}{\bar{\lambda}} \frac{\mathcal{L}^{-1}\left(\bar{\lambda}/\lambda_L\right)}{\mathcal{L}^{-1}\left(1/\lambda_L\right)}\left[F^2 - \frac{1}{F}\right], \tag{7}$$

and

$$\sigma_B = \frac{s\mu}{\bar{\lambda}_B^e} \frac{\mathcal{L}^{-1}\left(\bar{\lambda}_B^e/\lambda_L\right)}{\mathcal{L}^{-1}\left(1/\lambda_L\right)}\left[(F_B^e)^2 - \frac{1}{F_B^e}\right]. \tag{8}$$

In equations 7 and 8, s is a dimensionless material parameter specifying the shear modulus of network *B* relative to network *A*, μ is the shear modulus, λ_L is the limiting chain stretch, and $\mathcal{L}^{-1}(x)$ is the inverse of the Langevin function. The Langevin function given by $\mathcal{L}(x) = \coth(x) - 1/x$ and $\mathcal{L}^{-1}(x)$ is approximated by

$$\mathcal{L}^{-1}(\mathrm{x}) \approx \begin{cases} 1.31446\tan(1.58986\mathrm{x}) + 0.91209\mathrm{x}, & \text{if } |\mathrm{x}| < 0.84136 \\ 1/(\mathrm{sign}(\mathrm{x}) - \mathrm{x}, & \text{if } 0.84136 \le |\mathrm{x}| < 1 \end{cases}. \tag{9}$$

Strain stretch terms are given for both networks by

$$\bar{\lambda} = \sqrt{\frac{1}{3}\left[(F)^2 + \frac{2}{F}\right]} \tag{10}$$

and

$$\overline{\lambda_B^e} = \sqrt{\frac{1}{3}\left[(F_B^e)^2 + \frac{2}{F_B^e}\right]}. \tag{11}$$

The rate equation for viscous flow in network B is

$$\dot{\gamma}_B^v = \dot{\gamma}_0(\overline{\lambda_B^v} - 1 + \xi)^C \left[R\left(\frac{2|\sigma_B|}{3\tau_{base}} - \hat{\tau}_{cut}\right)\right]^m, \tag{12}$$

where

$$\overline{\lambda_B^v} = \sqrt{\frac{1}{3}\left[(F_B^v)^2 + \frac{2}{F_B^v}\right]}, \tag{13}$$

$\dot{\gamma}_0 = 1/s$ is a constant for dimensional consistency, *R(x) = (x + |x|)/2* is the ramp function, and $\hat{\tau}_{cut}$ is a cut-off stress below where no flow will occur. *C*, ξ, τ_{base}, and *m* are material constants.

With the viscous flow given in equation 12, the evolution of the viscoelastic deformation gradient (F_B) of network B is given by

$$\dot{F_B^v} = \dot{\gamma}_B^v \ \text{sign}[\sigma_B] F_B^v. \tag{14}$$

Uniaxial data from experiments were used to extract the optimum set of material parameters for the BB model that represent most of the experimental response fairly well. Material parameters for the BB model are given in table 2. Best material parameters were obtained by optimizing to reduce the errors using PolyUMod numerical routines (*15*). Since the BB model describes the behavior of the rubber well, incorporating the model directly into LSDYNA will be part of our future work.

Table 2. BB model constants for the neck rubber for different loading rate scenarios.

Model Parameter Description	**Case**	**A1 Impact Rates**	**B1 Blast Rates**	**C1 Auto Rates**	**A2 Impact Rates (+ Cyclic)**	**B2 Blast Rates (+ Cyclic)**	**C2 Auto Rates (+ Cyclic)**
	Model Constants	**2300, 1300, 500, 1/s**	**500, 1, 0.001/s**	**1,0.001/s**	**2300, 1300 500, 1/s, {E', E"}–freq**	**500, 1/, 0.001/s, {E', E"}–freq**	**1,0.001/s {E', E"}–freq**
Shear modulus of network A (MPa)	μ	1.22156	2.49584	2.17583	1.22156	2.17881	2.17583
Locking stretch	λ_L	6.05826	1.20723	1.18675	6.05826	1.15367	1.18675
Bulk modulus (MPa)	k	500	500	500	500	500	500
Stiffness of network B relative to A	s	28293.5	12.9004	7.21539	28293.5	9.5676	7.21683
Strain adjustment factor	ξ	0.01909	0.229882	0.317087	0.01909	0.337517	0.317087
Strain exponent	C	–1.71847	–0.97316	–1.01733	–1.71847	–0.95967	–1.01733
Flow resistance (MPa)	τ_{base}	3.93878	0.070253	0.296996	3.93878	0.693538	0.296996
Stress exponent	m	1.16972	1.11285	1.51296	1.16972	1.26362	1.51296
Normalized cut-off stress for flow	$\hat{\tau}_{cut}$	0.01	0.01	0.005	0.01	0.01	0.005
R^2 for goodness of fit	—	0.699	0.959	0.966	0.559	0.712	0.652

Table 2 provides BB model constants for six different loading rate scenarios (cases A1, B1, C1, A2, B2, and C2), with corresponding experimental data used for optimization to obtain the model constants. Appendix B shows the comparison of experimental data with what is being predicted by the model for these six different cases. We propose that case A1 or A2 model parameters to be used for impact events, where strain rates could be higher (A2 when cyclic loading is relevant). For blast events, we recommend that model parameters from either case B1 or B2 be used for numerical simulation (B2 when cyclic loading is relevant). For automotive crash events, model constants from cases C1 (or C2 when cyclic loadings are relevant) may be used. In this study, relaxation data were not used for calibration simulation due to additional issues associated with the convergence of the calibration simulations. The relaxation data has lower importance compared to monotonic loading rate, stress-strain data on actual numerical simulation of the events of interest. In the case of A2 with higher rates during cyclic loading, it was not possible to obtain an optimized calibration solution that would make predictions to also match reasonably well with DMA data in a reasonable time of calibration simulation. In general, optimized model constants reasonably predict the stress-strain response under monotonically increasing load compared to the cyclic small amplitude DMA experiments. For the loading scenarios of interest, such as a car crash and blast loading, monotonically increasing stress-strain data is more relevant. In future work, other viscoelastic materials from the HIII dummy, as well as other surrogate materials proposed for future generations of ATDs, will be investigated.

4. Conclusions

The rate dependence of the neck rubber used in the HIII ATD has been studied over a wide range of strain rates using different types of loading. Valid high-rate experiments were conducted to satisfy the requirements of constant strain rate and dynamic force equilibrium by carefully shaping the incident pulse of the loading device. The neck rubber was highly rate dependent by an order of magnitude increase in strength from quasi-static rate to high rate. Furthermore, the stress relaxation behavior was studied at quasi-static and intermediate rates, and the rubber was found to experience stress relaxation after being compressed to 43% strain and held for 300 s. In addition, frequency dependence response of storage and loss moduli at room temperature for the neck rubber was also studied for constitutive modeling so that the models would be valid for most possible types of loading sequences. After exploring many constitutive models in literature, it was found that compared to all other models, the BB model represented the experimental data reasonably well. We hope to work with the LSDYNA Company to incorporate this model into the LSDYNA numerical code.

5. References

1. North Atlantic Treaty Organization. *Anthropomorphic Dummies for Crash and Escape System Testing; Aerospace Medical Panel of AGARD*. Canada Communication Group: Hull (Quebec), Canada, July 1996.
2. Chen, W.; Zhang, B.; Forrestal, M. J. A Split Hopkinson Bar Technique for Low Impedance Materials. *Experimental Mechanics* **1999**, *39*, 81–85.
3. Song, B.; Chen, W. Dynamic Stress Equilibration in Split Hopkinson Pressure Bar Tests on Soft Materials. *Experimental Mechanics* **2004**, *44*, 300–312.
4. Song, B.; Chen, W. Loading and Unloading SHPB Pulse Shaping Techniques for Dynamic Hysteretic Loops. *Experimental Mechanics* **2004**, *44*, 622–627.
5. Song, B.; Chen, W. One-Dimensional Dynamic Compressive Behavior of EPDM Rubber. *Journal of Engineering Materials and Technology* **2003**, *125*, 294–301.
6. Lee, O. S.; Cho, K. S.; Kim, S. H.; Han, Y. H. Dynamic Deformation Behavior of Soft Material Using SHPB Technique With Pulse Shaper. *International Journal of Modern Physics B* **2006**, *20* (25n27).
7. Hybrid III 50th Neck Service Bulletin. www.humaneticsatd.com (accessed 19 October 2012).
8. Chen, W.; Song, B. *Split Hopkinson (Kolsky) Bar*; Springer: New York, NY, 2010.
9. Warren, T. L.; Forrestal, M. J. Comments on the Effect of Radial Inertia in the Kolsky Bar Test for an Incompressible Material. *Experimental Mechanics* **2010**, *50* (8), 1253–1255.
10. Song, B.; Syn, C. J.; Grupido, C. L.; Chen, W.; Lu, W. Y. A Long Split Hopkinson Pressure Bar (LSHPB) for Intermediate Rate Characterization of Soft Materials. *Experimental Mechanics* **2008**, *48*, 809–815.
11. Bergstrom, J. S.; Boyce, M. C. Constitutive Modeling of the Large Strain Time-Dependent Behavior of Elastomers. *J. Mech. Phys. Solids* **1998**, *46*, 931–954.
12. Arruda, E. M.; Boyce, M. C. A Three-Dimensional Constitutive Model for the Large Stretch Behavior of Rubber Elastic Materials. *J. Mech. Phys. Solids* **1993**, *41* (2), 389–412.
13. Bergstrom, J. S.; Boyce, M. C. Mechanical Behavior of Particle Filled Elastomers. *Rubber Chem. Technol.* **1999**, *72*, 633–656.

14. Bergstrom, J. S.; Boyce, M. C. Large Strain Time-Dependent Behavior of Filled Elastomers. *Mechanics of Materials* **2000**, *32*, 620–644.

15. Veryst Engineering. *PolyUMod™ User Manual*; version 2.1.9. Needham Heights, MA, 2012.

INTENTIONALLY LEFT BLANK.

Appendix A. Experimental Data

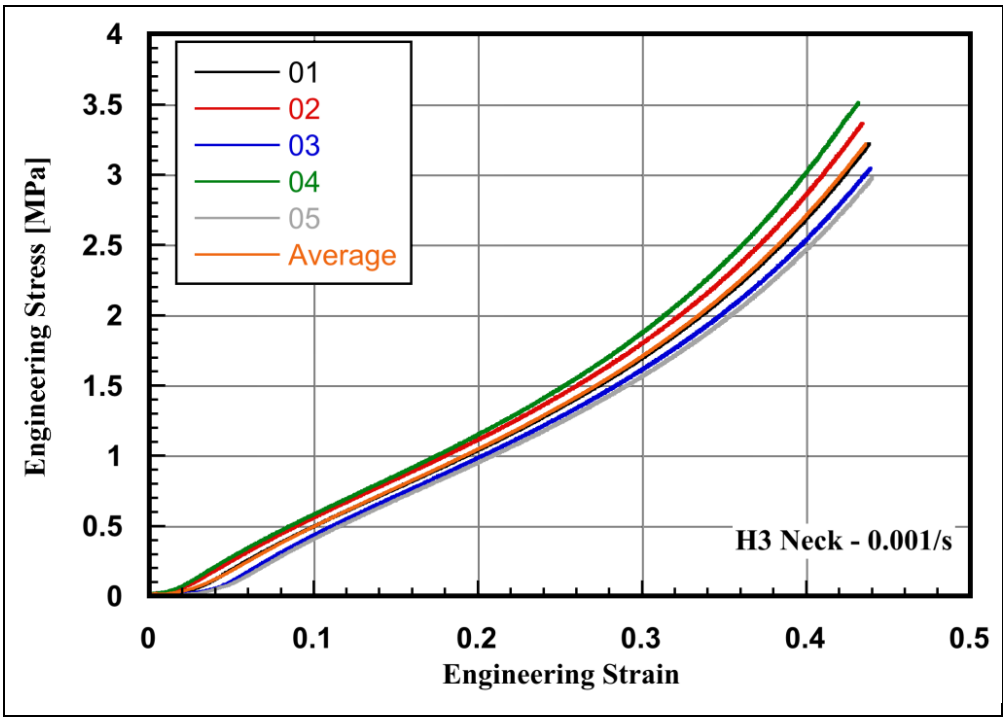

Figure A-1. Engineering stress-strain behavior of the Hybrid III (HIII) neck rubber at the quasi-static strain rate.

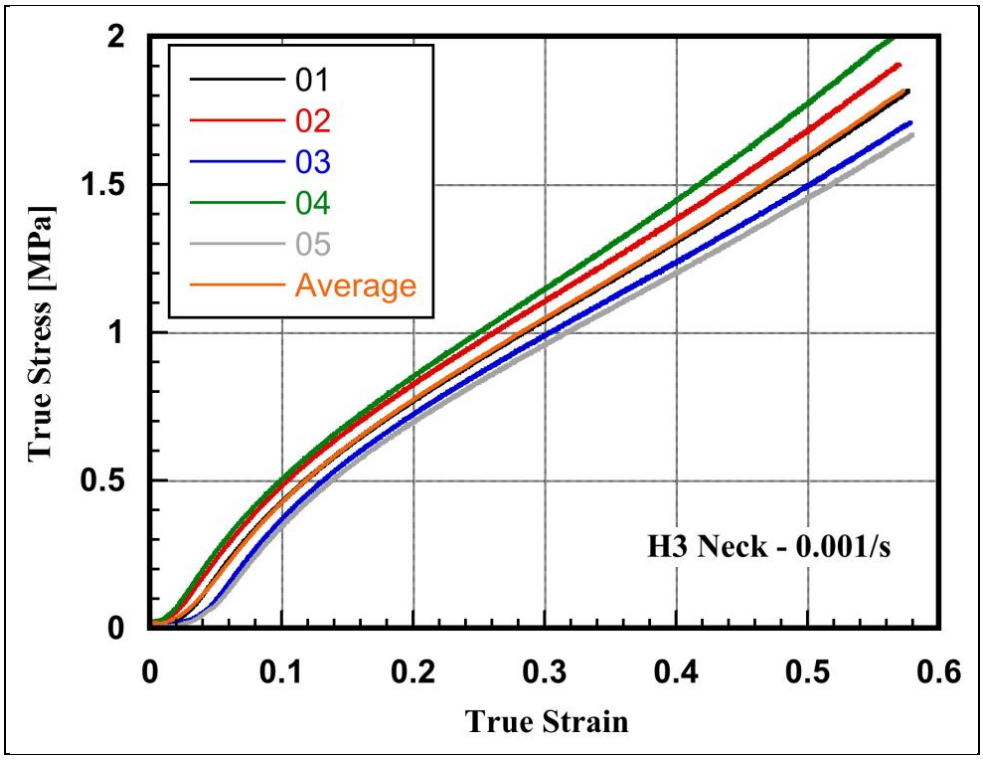

Figure A-2. True stress-strain behavior of the HIII neck rubber at the quasi-static strain rate.

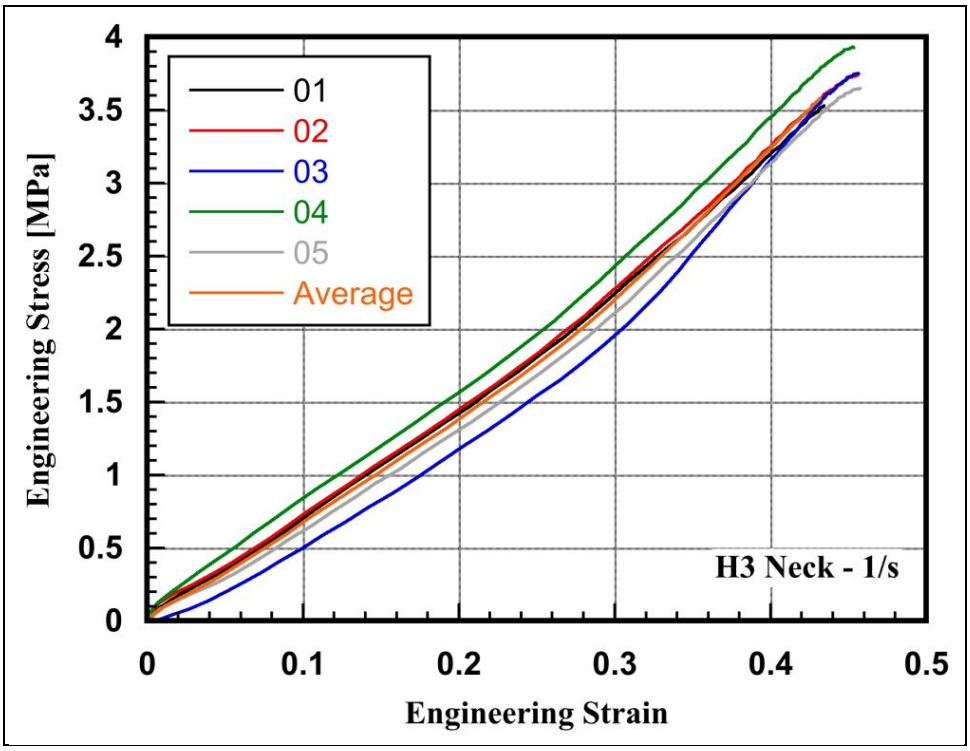

Figure A-3. Engineering stress-strain behavior of the HIII neck rubber at the intermediate strain rate.

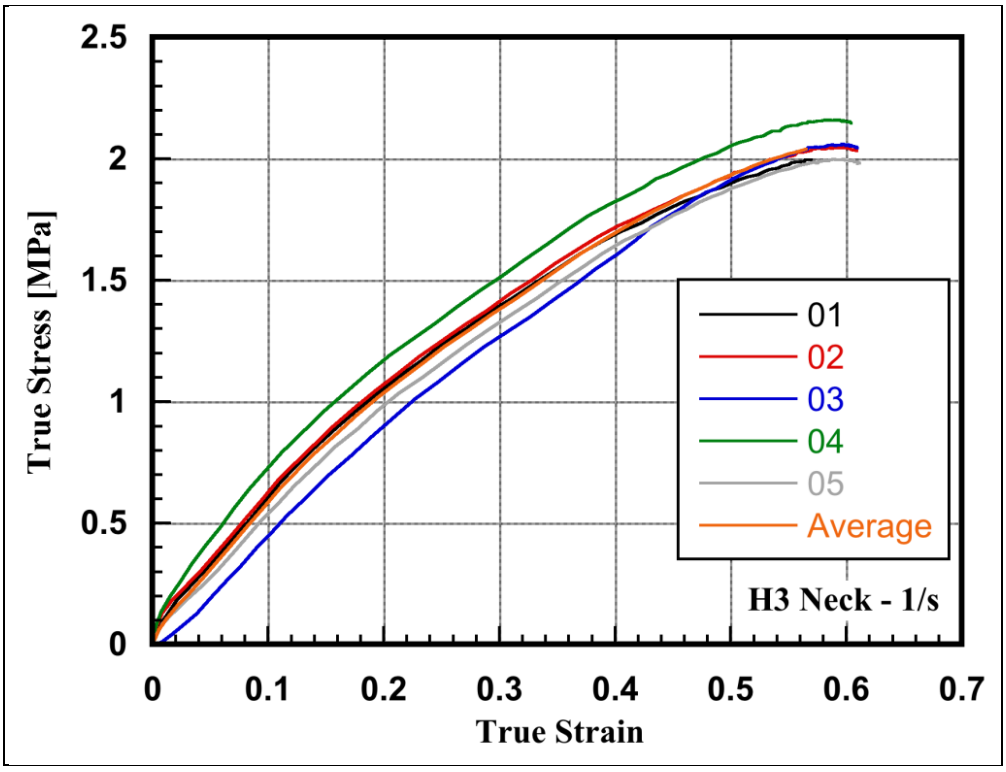

Figure A-4. True stress-strain behavior of the HIII neck rubber at the intermediate strain rate.

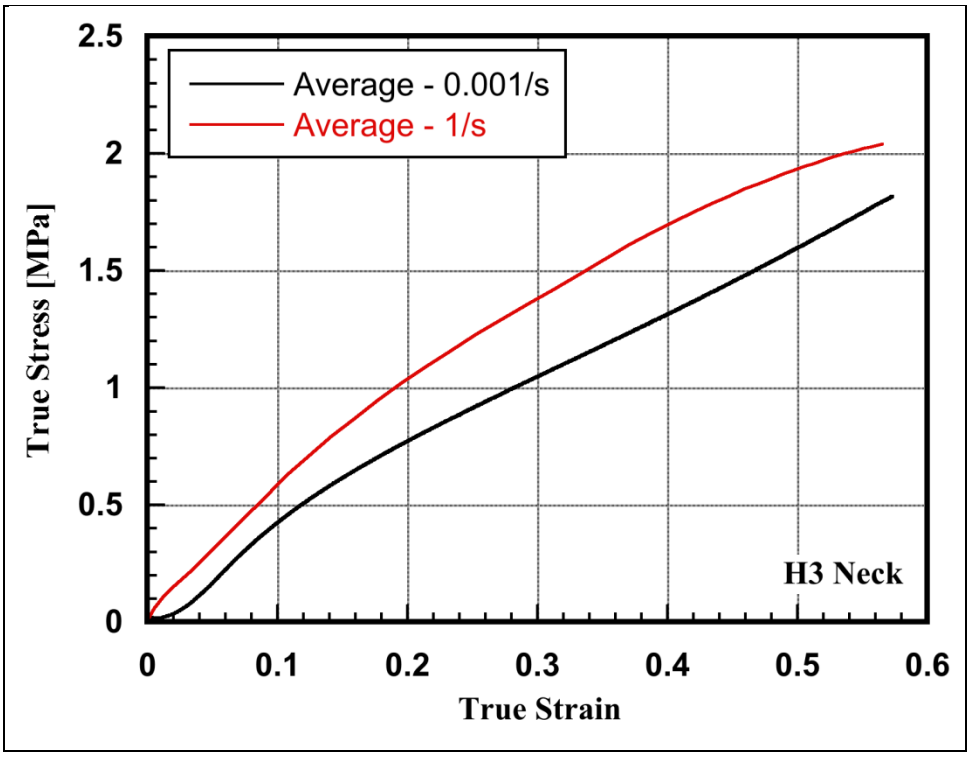

Figure A-5. Average true stress-strain behavior of the neck rubber at the quasi-static and intermediate rates.

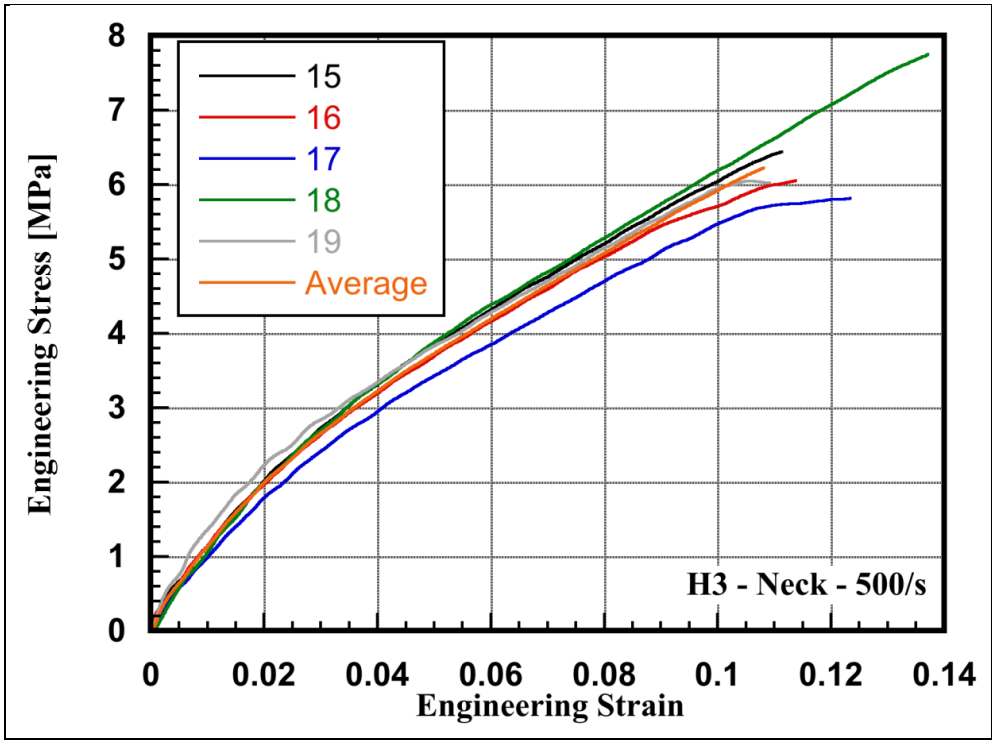

Figure A-6. Engineering stress-strain behavior of the neck rubber at 500 s-1.

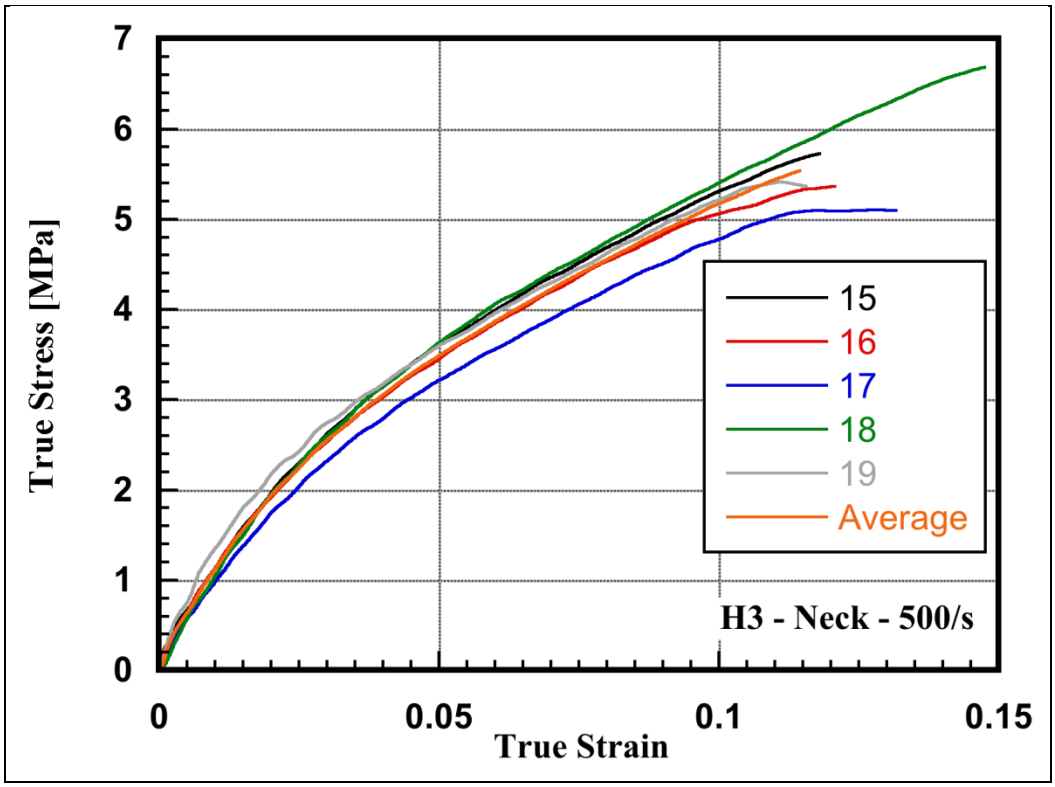

Figure A-7. True stress-strain behavior of the neck rubber at 500/s.

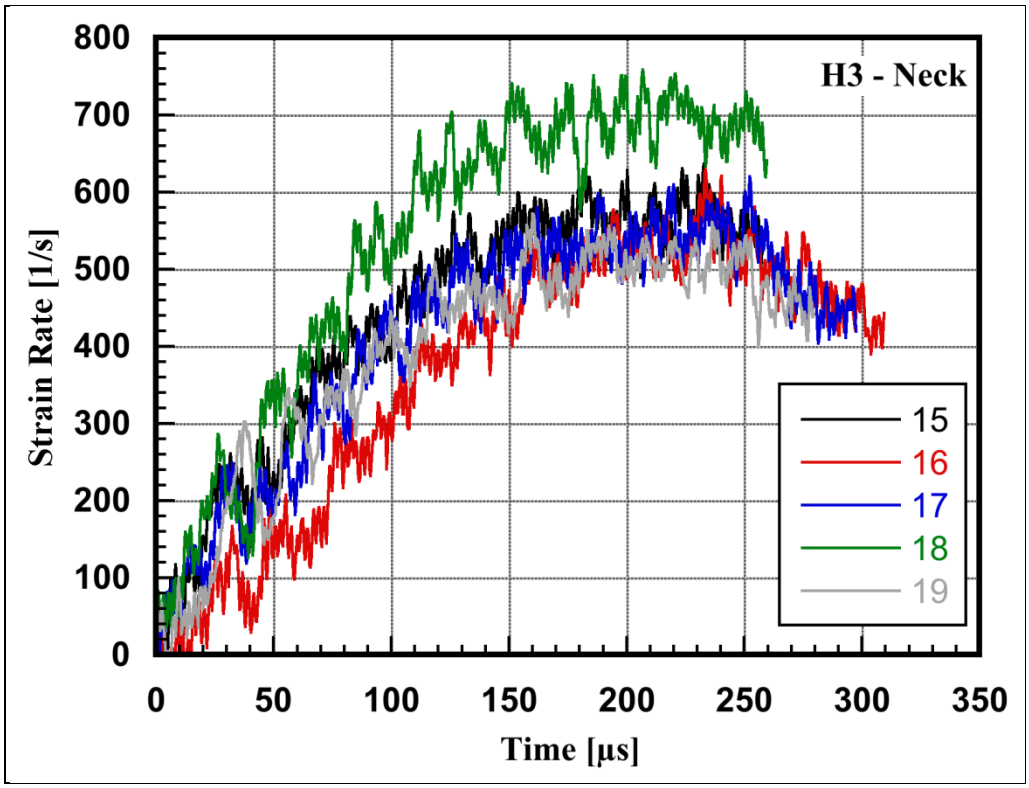

Figure A-8. Strain rate histories from 500/s experiments.

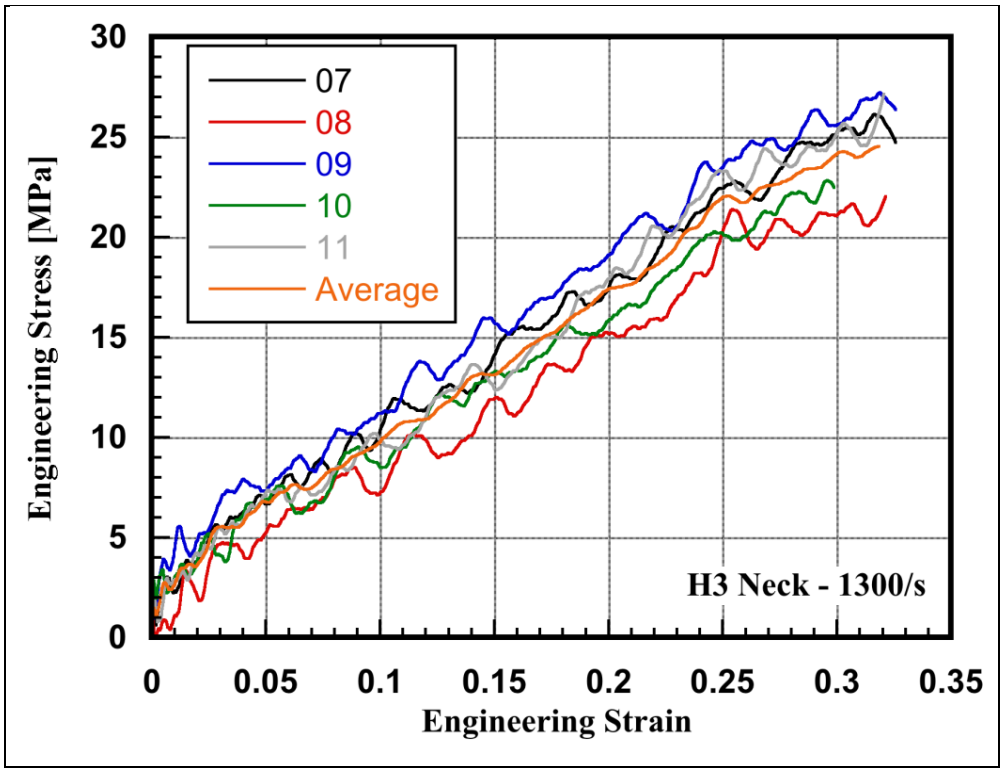

Figure A-9. Engineering stress-strain behavior of the HIII neck rubber at a strain rate of 1300/s.

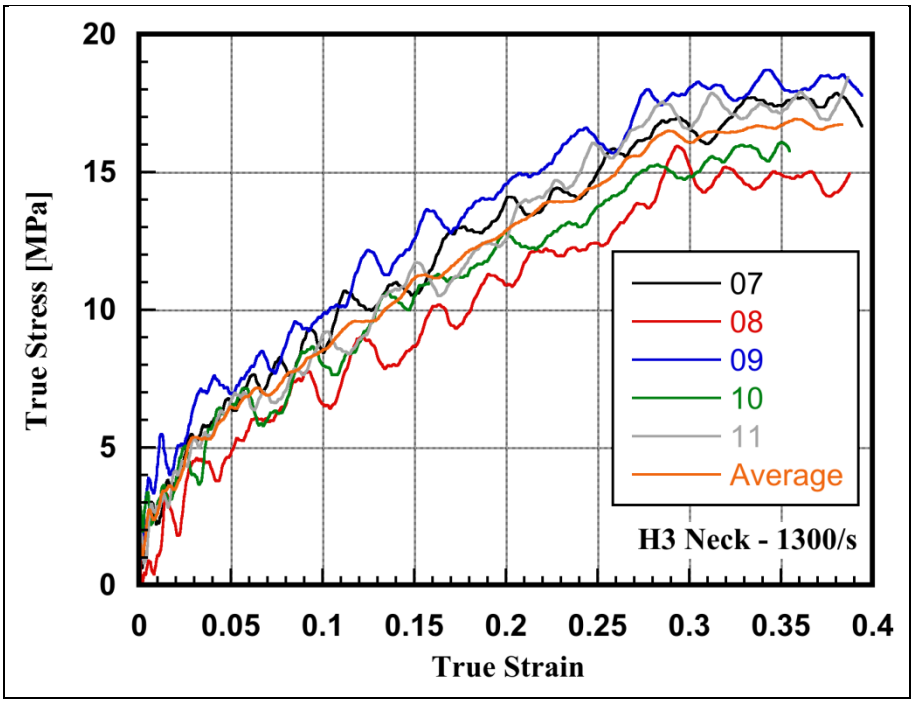

Figure A-10. True stress-strain behavior of the HIII neck rubber at a strain rate of 1300/s.

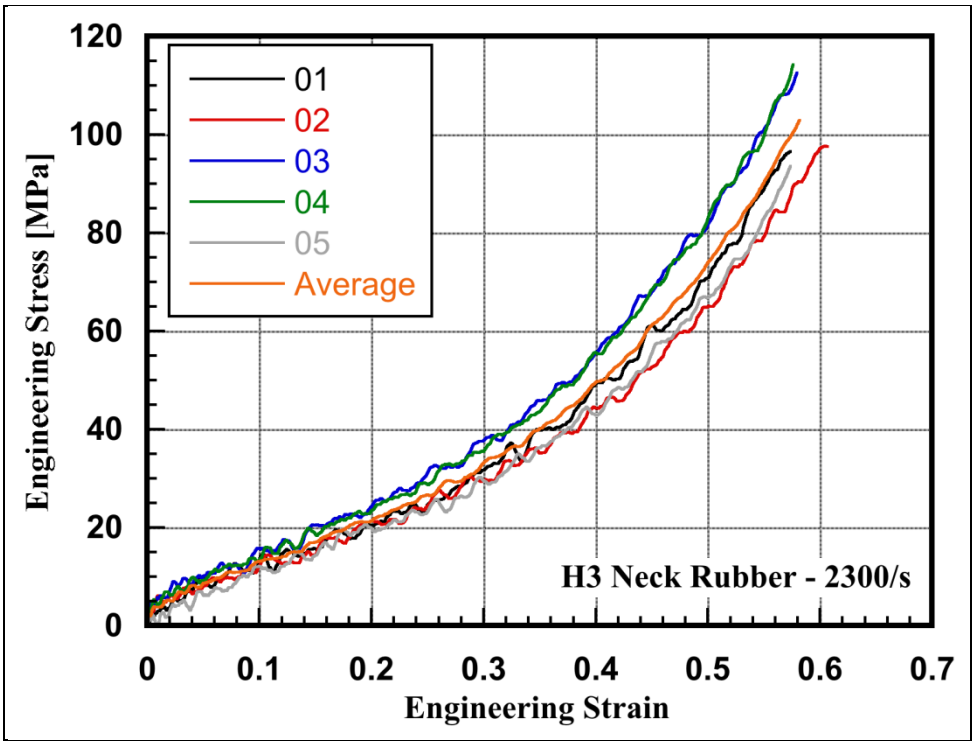

Figure A-11. Engineering stress-strain behavior of the HIII neck rubber at a strain rate of 2300/s.

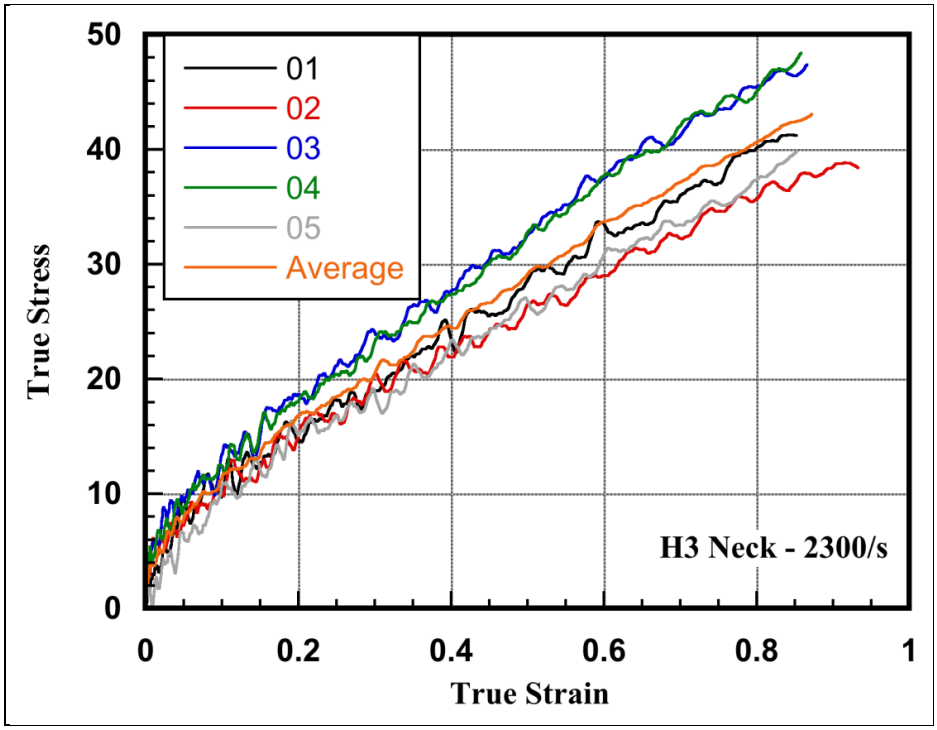

Figure A-12. True stress-strain behavior of the HIII neck rubber at a strain rate of 2300/s.

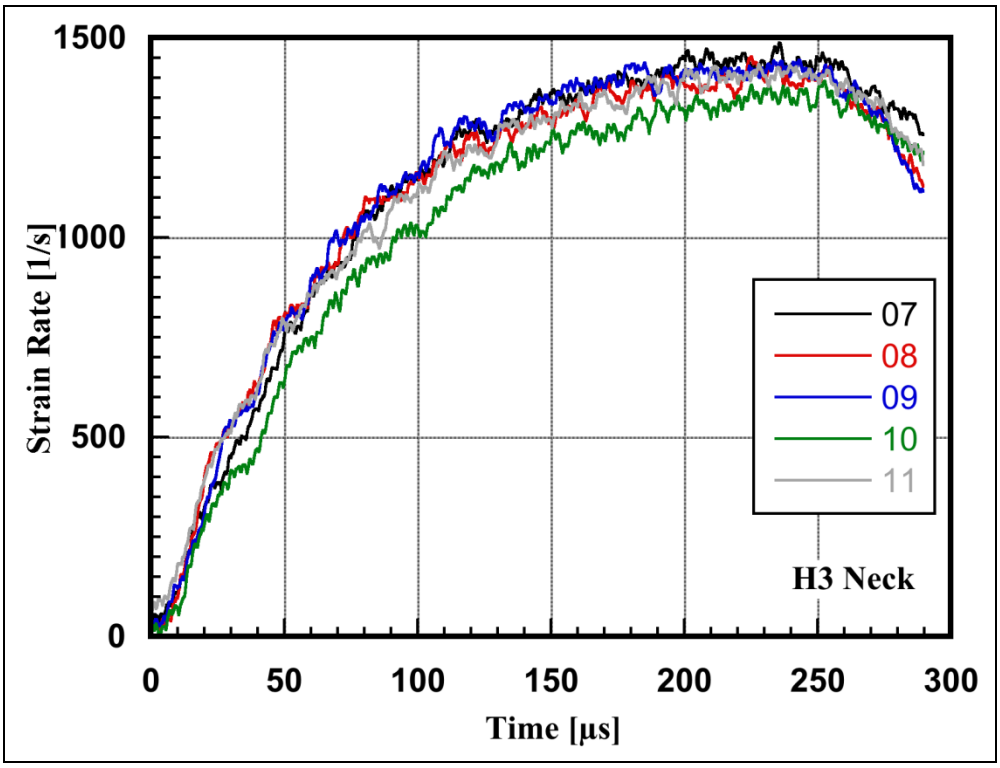

Figure A-13. Strain rate histories from 1300/s experiments.

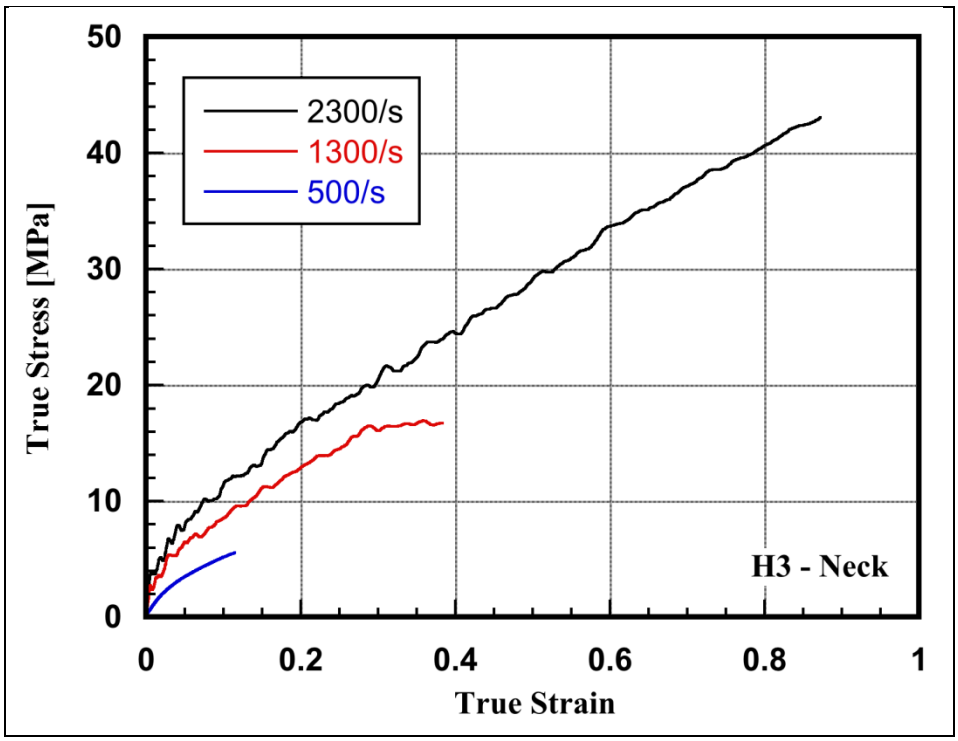

Figure A-14. True stress-strain behavior of the HIII neck rubber at high strain rate.

Appendix B. Bergstrom-Boyce (BB) Model Predictions Compared With Corresponding Experimental Data

B.1 Case A1: 1, 500, 1300, and 2300/s High-Rate, Biased Model

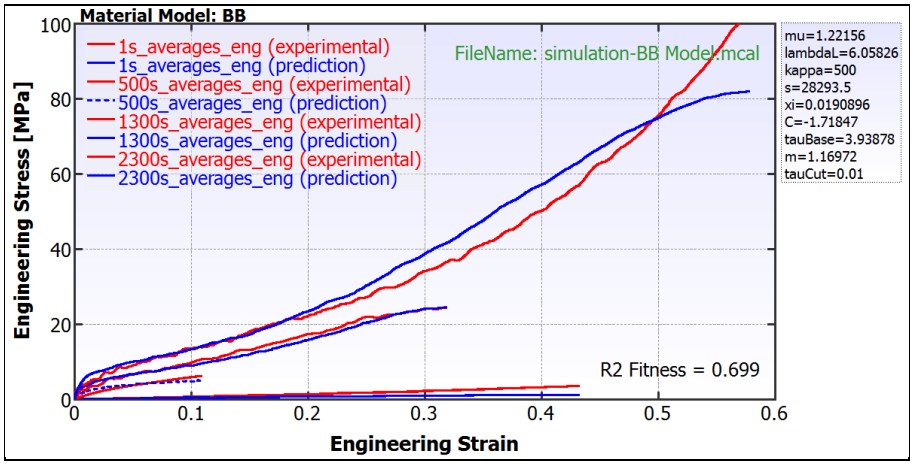

Figure B-1. Comparison of the BB model prediction with case A1 – higher rate (1–2300/s), biased experimental stress-strain data.

B.2 Case A2: 1, 500, 1300, and 2300/s High-Rate, Biased Model With Dynamic Mechanical Analysis (DMA) Vibratory Response

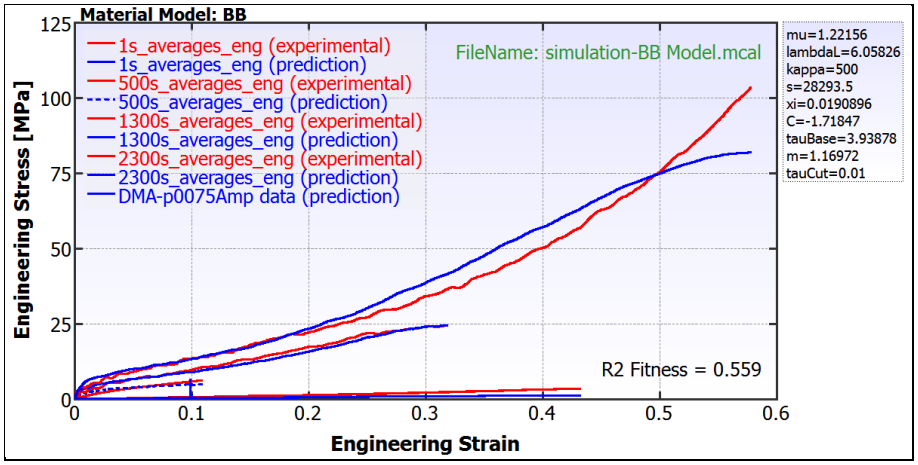

Figure B-2. Comparison of the BB model prediction with case A2 – higher rate (1–2300/s), biased experimental stress-strain data with DMA vibratory data.

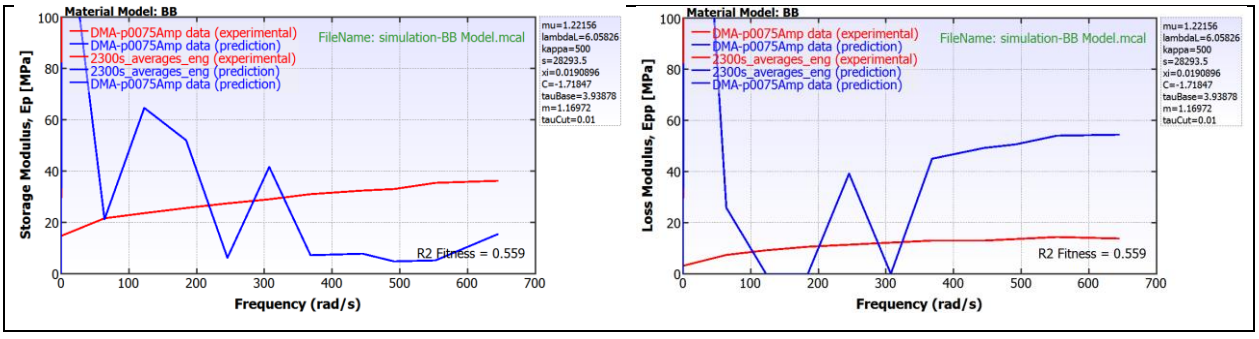

Figure B-3. Comparison of the BB model prediction with case A2 – DMA vibratory storage and loss moduli data.

B.3 Case B1: 0.001, 1, and 500/s Lower Rate, Biased Model

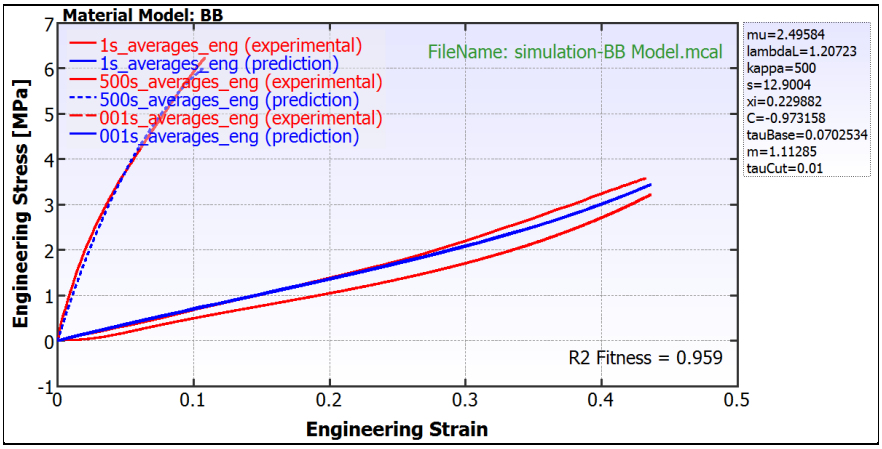

Figure B-4. Comparison of the BB model prediction with case B1 – lower rate (0.001–500/s), biased experimental stress-strain data.

B.4 Case B2: 0.001, 1, and 500/s High-Rate, Biased Model With DMA Vibratory Response

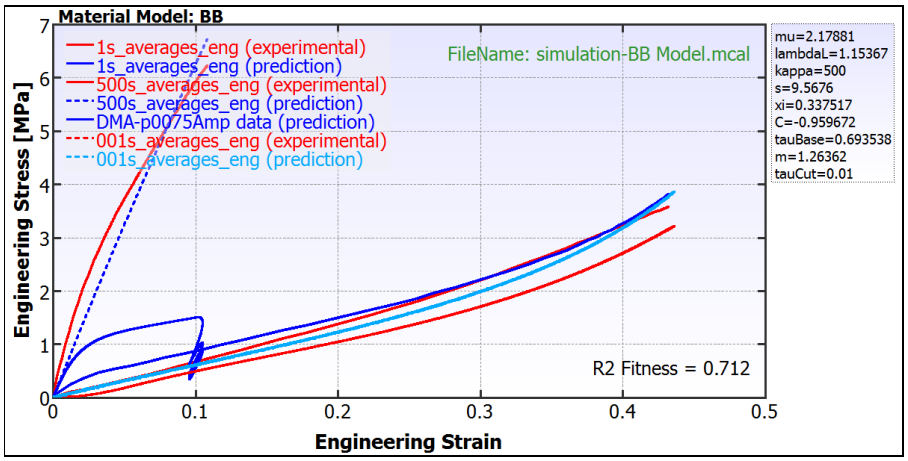

Figure B-5. Comparison of the BB model prediction with case B2 – lower rate (0.001–500/s), biased experimental stress-strain data with DMA vibratory data.

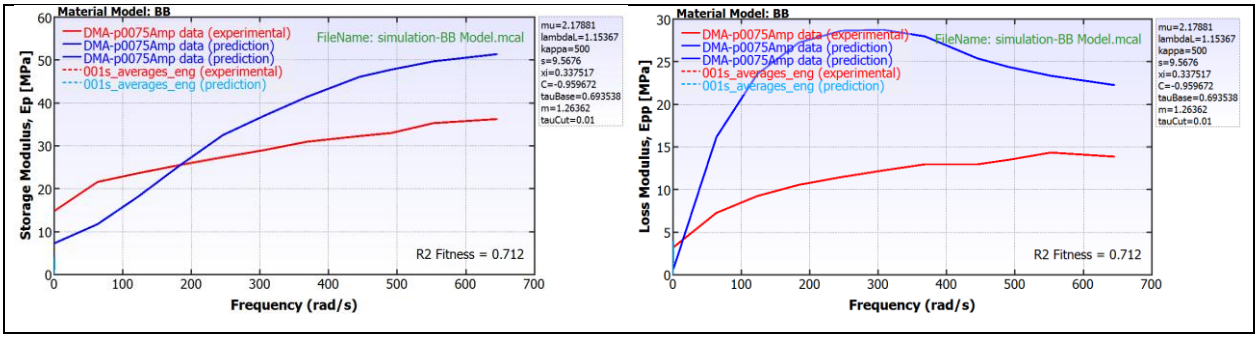

Figure B-6. Comparison of the BB model prediction with case B2 – DMA vibratory storage and loss moduli data.

B.5 Case C1: 0.001 and 1/s Lower Rate, Biased Model

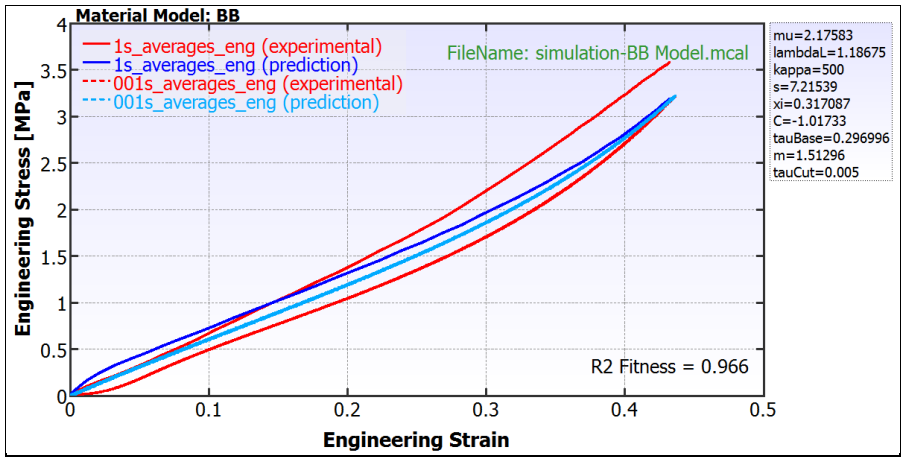

Figure B-7. Comparison of the BB model prediction with case C1 – lower rate (0.001–500/s), biased experimental stress-strain data.

B.6 Case C2: 0.001, 1/s High-Rate, Biased Model With DMA Vibratory Response

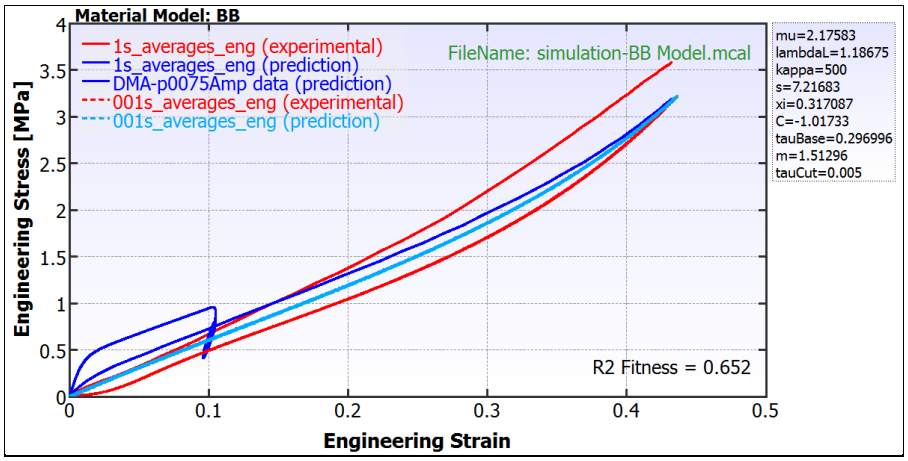

Figure B-8. Comparison of the BB model prediction with case C2 – lower-rate (0.001–500/s), biased experimental stress-strain data with DMA vibratory data.

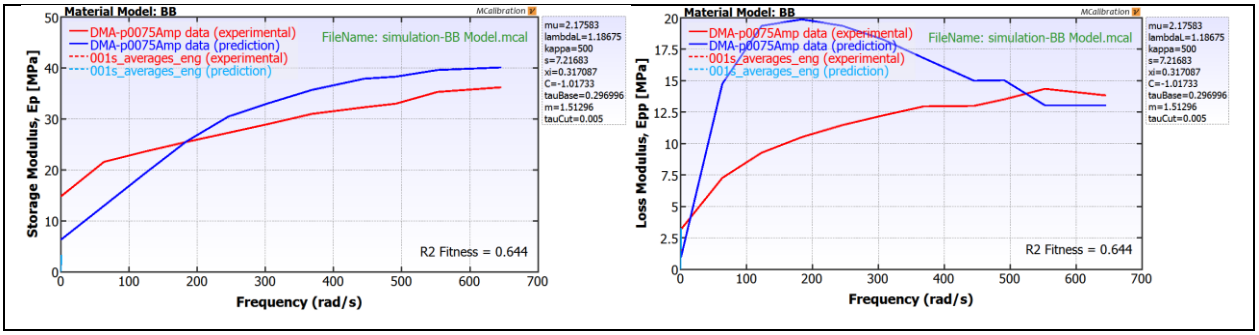

Figure B-9. Comparison of the BB model prediction with case C2 – DMA vibratory storage and loss moduli data.

NO. OF COPIES ORGANIZATION

1 (PDF only) DEFENSE TECHNICAL INFORMATION CTR
DTIC OCA
8725 JOHN J KINGMAN RD
STE 0944
FORT BELVOIR VA 22060-6218

1 DIRECTOR
US ARMY RESEARCH LAB
IMAL HRA
2800 POWDER MILL RD
ADELPHI MD 20783-1197

1 DIRECTOR
US ARMY RESEARCH LAB
RDRL CIO LL
2800 POWDER MILL RD
ADELPHI MD 20783-1197

1 US ARMY RESEARCH OFFICE
RDRL ROE M
D STEPP
PO BOX 12211
RESEARCH TRIANGLE PARK
NC 27709-2211

1 US ARMY RESEARCH OFFICE
RDRL ROE V
L RUSSELL
BLDG 205
ADELPHI MD 20783-1197

1 HUMAN SYS DEPT
B SHENDER
CODE 4656 BLDG 2187 STE 2280A
NVL AIR WARFARE CTR
AIRCRAFT DIV
48110 SHAW RD UNIT 5
PATUXENT RIVER MD 20670-1906

2 DEPT OF MECHANICAL ENGRG
THE JOHNS HOPKINS UNIV
LATROBE 122
K T RAMESH
V NGUYEN
3400 N CHARLES ST
BALTIMORE MD 21218

1 UNIV OF TEXAS-AUSTIN
ARSPC ENGRG & ENGRG MECH
K RAVI-CHANDAR
1 UNIV STATION C0600
AUSTIN TX 78712-0235

NO. OF COPIES ORGANIZATION

4 JTAPIC PROGRAM OFC
US ARMY MEDICAL RSRCH & MATERIEL CMND
MRMC RTB
J USCILOWICZ
W LEI
F LEBEDA
R GUPTA
504 SCOTT ST
FORT DETRICK MD 21702-5012

1 NAVEL SURFACE WARFARE CTR
CODE 664
P DUDT
9500 MACARTHUR DR
WEST BETHESDA MD 20817

1 TARDEC
RDTA RS
R SCHERER
BLDG 200C RM 1150
WARREN MI 48397

1 NATICK SOLDIER RSRCH DEV & ENGRG CTR
AMSRD NSC WS TB
M G CARBONI
KANSAS ST
BLDG 4 RM 247
NATICK MA 01760-5000

1 NATICK SOLDIER RSRCH DEV & ENGRNG CTR
RDNS D
M CODEGA
KANSAS ST
NATICK MA 01760

1 NATICK SOLDIER RSRCH DEV & ENGRNG CTR
RDNS WPW P
R DILALLA
KANSAS ST
NATICK MA 01760

1 NATICK SOLDIER RSRCH DEV & ENGRNG CTR
RNDS TSM
M STATKUS
KANSAS ST
NATICK MA 01760

NO. OF
COPIES ORGANIZATION

3 NATICK SOLDIER RSRCH DEV & ENGRNG CTR
RDNS WSD B
J WARD
P CUNNIFF
M MAFFEO
KANSAS ST
NATICK MA 01760

2 SOUTHWEST RSRCH INST
MECHL & MTRL ENGRG DIV
MTRL ENGRNG DEPT
D NICOLELLA
W FRANCIS
6220 CULEBRA RD
SAN ANTONIO TX 78238

1 SANDIA NATIONAL LAB
PO BOX 969 MS 9404
B SONG
LIVERMORE CA 94551-0969

1 THE UNIV OF UTAH
50 S CENTRAL CAMPUS DR
K L MONSON
2132 MERRILL ENGRG BLDG
SALT LAKE CITY UT 84112

1 COLUMBIA UNIV
351 ENGRG TERRACE
B MORRISON
1210 AMSTERDAM AVE
MAIL CODE 8904
NEW YORK NY 10027

1 APPLIED RSRCH ASSOC INC
SOUTHWEST DIV
C E NEEDHAM
4300 SAN MATEO BLVD NE
STE A-220
ALBUQUERQUE NM 87110

2 CENTER FOR INJURY BIOMECHANICS
WAKE FOREST UNIV
J STITZEL
F S GAYZIK
MEDICAL CTR BLVD
WINSTON-SALEM NC 27157

NO. OF
COPIES ORGANIZATION

1 THE AIR FORCE RSRCH LAB
AFRL/MLLMP
T TURNER
BLDG 655 RM 115
2230 TENTH ST
WRIGHT-PATTERSON AFB
OH 45433-7817

3 NATL GROUND INTLLGNC CTR
D EPPERLY
T SHAVER
T WATERBURY
2055 BOULDERS RD
CHARLOTTESVILLE VA 22911-8318

2 SOUTHWEST RESEARCH INST
T HOLMQUIST
G JOHNSON
5353 WAYZATA BLVD STE 607
MINNEAPOLIS MN 55416

1 AIR FORCE RSRCH LAB
AFRL RWMW
B MARTIN
EGLIN AFB FL 32542

2 HUMANETICS
J WANG
H PANG
47460 GALLEON DR
PLYMOUTH MI 48170

4 DRDC VALCARTIER
K WILLIAMS
A BOUAMOUL
L MARTINEAU
D NANDLALL
2459 PIE-XI BLVD N
QUEBEC QC G3J 1X5
CANADA

1 DRDC TORONTO
C BURRELL
PO BOX 2000
1133 SHEPPARD AVE WEST
TORONTO ON M3M 3B9
CANADA

NO. OF
COPIES ORGANIZATION

1 HUMAN PROTECTION &
PERFORMANCE DIV
DEFENCE SCI AND TECHLGY
ORGANISATION
DEPT OF DEFENCE
T RADTKE
BLDG 109 506 LORIMER ST
FISHERMANS BEND VICTORIA 3207
AUSTRALIA

1 DEFENCE SCI & TECHLGY
ORGANISATION
S WECKERT
PO BOX 1500
EDINBURGH SA 5111
AUSTRALIA

ABERDEEN PROVING GROUND

1 US ARMY ABERDEEN TEST CTR
TEDT AT SLB
A FOURNIER
400 COLLERAN RD
APG MD 21005-5059

115 DIR USARL
RDRL CIH C
P CHUNG
RDRL HRS C
W HAIRSTON
B LANCE
K MCDOWELL
K OIE
J VETTEL
RDRL SL
R COATES
RDRL SLB A
B WARD
RDRL SLB W
A BREUER
N EBERIUS
P GILLICH
C KENNEDY
A KULAGA
W MERMAGEN
K RAFAELS
L ROACH
R SPINK
M TEGTMEYER
RDRL WM
P BAKER
B FORCH
S KARNA
J MCCAULEY

NO. OF
COPIES ORGANIZATION

P PLOSTINS
RDRL WML
M ZOLTOSKI
RDRL WMS
M VANLANDINGHAM
RDRL WML A
W OBERLE
RDRL WML F
G BROWN
RDRL WML G
J SOUTH
RDRL WML H
T EHLERS
M FERMEN-COKER
L MAGNESS
C MEYER
J NEWILL
D SCHEFFLER
S SCHRAML
B SCHUSTER
RDRL WMM
B DOWDING
J BEATTY
RDRL WMM A
D O'BRIEN
R EMERSON
E WETZEL
RDRL WMM B
R CARTER
B CHEESEMAN
G GAZONAS
B LOVE
P MOY
C RANDOW
C YEN
RDRL WMM C
A BUJANDA
R JENSEN
J LA SCALA
J YIM
RDRL WMM D
E CHIN
S WALSH
W ZIEGLER
RDRL WMM E
G GILDE
J LASALVIA
P PATEL
J SINGH
J SWAB
RDRL WMM F
S GRENDAHL
L KECSKES
E KLIER

NO. OF
COPIES ORGANIZATION

RDRL WMM G
J LENHART
R MROZEK
A RAWLETT
K STRAWHECKER
RDRL WMP
S SCHOENFELD
RDRL WMP B
A DAGRO
A DWIVEDI
A GUNNARSSON
C HOPPEL
M LYNCH
D POWELL
B SANBORN (5 CPS)
S SATAPATHY
M SCHEIDLER
T WEERASOORIYA (5 CPS)
RDRL WMP C
R BECKER
S BILYK
T BJERKE
J BRADLEY
D CASEM
J CLAYTON
D DANDEKAR
M GREENFIELD
B LEAVY
C MEREDITH
M RAFTENBERG
C WILLIAMS
RDRL WMP D
R DONEY
D KLEPONIS
J RUNYEON
B SCOTT
B VONK
RDRL WMP E
S BARTUS
M BURKINS
D HACKBARTH
T JONES
RDRL WMP F
E FIORAVANTE
A FRYDMAN
N GNIAZDOWSKI
R GUPTA
R KARGUS
C CUMMINS
RDRL WMP G
N ELDREDGE
S KUKUCK